Analytical Solutions for Uniaxial-Film-Compensated Wide-View Liquid Crystal Displays

Xinyu Zhu, Zhibing Ge, *Student Member, IEEE*, and Shin-Tson Wu, *Fellow, IEEE*

Invited Paper

***Abstract*—The uniaxial-film-compensated wide-view liquid crystal displays, with initially homogeneous alignment and vertical alignment, are analyzed. For each compensation scheme, the analytical solutions with the illustration of Poincaré sphere representation are derived. Based on the analytical solutions, the 100:1 iso-contrast contours at any viewing angle can be easily achieved for most of the compensation schemes.**

***Index Terms*—Analytical solutions, film compensation, fringe-field switching (FFS), in-plane switching (IPS), liquid crystal display (LCD), multi-domain vertical alignment (MVA), patterned vertical alignment (PVA), wide viewing angle (WVA).**

I. Introduction

WIDE VIEWING angle (WVA) is a critical requirement for high-end liquid crystal displays (LCDs), such as high definition televisions and large-screen desktop monitors. The conventional twisted-nematic (TN) LCD [1] exhibits a narrow and asymmetric viewing cone because the liquid crystal (LC) directors are tilted up under applied voltage so that the incident light experiences different effective birefringence when viewed from different oblique angles. To achieve WVA, a good dark state within a large viewing cone has to be maintained. So far, two types of LC alignments have been commonly used for this purpose: homogeneous alignment and vertical alignment.

The popular display modes with initially homogeneous alignment are in-plane switching (IPS) [2], [3] and fringe-field switching (FFS) [4]. In these modes, the LC layer is homogeneously aligned between two holding substrates and switched within the plane parallel to the substrates by the interdigital electrodes. Because of the in-plane reorientation of LC molecules, the effective birefringence viewed from opposite oblique angles is the same. As a result, the viewing angle is wide and symmetric. In the category of initially vertical alignment, multi-domain vertical alignment (MVA) [5] and patterned vertical alignment PVA) [6] are two representative examples. In both MVA and PVA modes, an LC layer with negative dielectric anisotropy $(\Delta\varepsilon < 0)$ is aligned vertically between two supporting substrates and switched to form multiple domains by the fringe electric field which is generated by either electrode protrusions or patterned electrodes, rendering symmetric viewing characteristics.

A common feature of IPS, FFS, MVA, and PVA modes is that the LC cell is sandwiched between two crossed linear polarizers. At normal incidence, the LC layer in the voltage-off state does not modulate the polarization state of the incident linearly polarized light from the entrance polarizer. As a result, a good dark state is achieved since this linearly polarized light is completely absorbed by the crossed analyzer. However, at oblique angles the incident light leaks through the crossed polarizers, especially at the bisectors. This light leakage stems from two factors. First, the absorption axes of the crossed polarizers are no longer orthogonal to each other under off-axis oblique view. As a result, the extinction ratio of these two crossed polarizers decreases and light leakage occurs. Second, in some cases, due to the effective birefringence effect of the LC layer the obliquely incident linearly polarized light is modulated and it becomes elliptically polarized after traversing through the LC layer. Consequently, the analyzer can not completely absorb the elliptically polarized light leading to light leakage at off-axis. This light leakage in the dark state deteriorates the contrast ratio and thereby degrades the viewing angle performance.

To suppress the light leakage at oblique angles and further widen the viewing angle, several phase compensation schemes using uniaxial films [7]–[9] and biaxial films [10]–[12] have been proposed. Computer simulation and experimental results have been reported, but the rigorous analytical solutions have not been published. The objective of this paper is to provide comprehensive analytical solutions for the mainstream uniaxial-film-compensated WVA LCDs. With the analytical solutions, the inter-dependency between LC cell and film parameters can be clearly revealed. More importantly, analytical solutions provide a clear physical description about the compensation mechanisms.

In the following sections, we first analyze the phase compensation principles using Poincaré sphere representation [13]. Then, we systematically derive the analytical solutions for some commonly employed IPS and MVA modes.

II. Principles of Uniaxial Film Compensation

Before we begin the detailed film compensation scheme for each mainstream WVA LCD, let us review some underlying theoretical bases for better understanding the principles of film

Manuscript received September 27, 2005; revised November 11, 2005. This work is supported by Toppoly Optoelectronics Corporation (Taiwan), Chu-Nan, Taiwan, R.O.C.

X. Zhu and S.-T. Wu are with the College of Optics and Photonics, University of Central Florida, Orlando, FL 32816 USA (e-mail: xzhu@mail.ucf.edu; swu@mail.ucf.edu).

Z. Ge is with the Department of Electrical and Computer Engineering, University of Central Florida, Orlando, FL 32816 USA (e-mail: zge@mail.ucf.edu).

Digital Object Identifier 10.1109/JDT.2005.863599

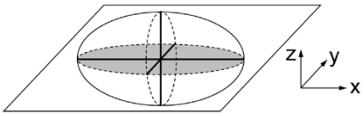

Fig. 1. Refractive index ellipsoid of a uniaxial medium.

TABLE I
REFRACTIVE INDEX RELATIONSHIP OF UNIAXIAL FILMS

Film type	Refractive index relationship
Positive a-film	$n_e \equiv n_x > n_y = n_z \equiv n_o$
Negative a-film	$n_e \equiv n_x < n_y = n_z \equiv n_o$
Positive c-film	$n_o \equiv n_x = n_y < n_z \equiv n_e$
Negative c-film	$n_o \equiv n_x = n_y > n_z \equiv n_e$

compensation. These theories include: 1) uniaxial film classification; 2) phase retardation of uniaxial media at oblique incidence; 3) Poincaré sphere representation; and 4) cause of light leakage of crossed polarizers under oblique view.

A. Uniaxial Film Classification

Uniaxial film is an anisotropic birefringent film with only one optical axis. For simplicity, we limit our discussions to those nonabsorption uniaxial films only. Fig. 1 shows the refractive index ellipsoid of a uniaxial film. The shadow plane represents the film's surface plane, which is parallel to the x-y plane. From the viewpoint of optical axis orientation, uniaxial films can be classified into : 1) a-film and 2) c-film. An a-film's optical axis is parallel to the film surface, while a c-film's optical axis is perpendicular to the film surface.

Both the a-film and c-film can be further divided into positive or negative films depending on the relative values of the extraordinary refractive index n_e and the ordinary refractive index n_o. Table I lists all four uniaxial films and their refractive index relationships. As a general rule, a positive uniaxial film means $n_e > n_o$, otherwise, $n_e < n_o$ for a negative uniaxial film.

B. Phase Retardation of Uniaxial Media at Oblique Incidence

Both the uniaxial compensation film and nematic LC layer can be treated as uniaxial media. When a light propagates into a uniaxial film, generally two forward eigenwaves (one ordinary wave and one extraordinary wave) are evoked within the medium. After the light passing through the uniaxial medium, phase retardation occurs between these two eigenwaves. Fig. 2 shows an arbitrary oblique incident light with an incident angle θ_0 propagates in a uniaxial medium. Here, the x-y plane is chosen to be parallel to the medium layer surface and z-axis is along the surface normal. In the chosen coordinates system, the incident plane forms an angle ϕ_0 with respect to the x-axis. The optical axis of the uniaxial medium is oriented at tilt angle θ_n and azimuthal angle ϕ_n, and the extraordinary and ordinary refractive indices of the uniaxial medium are n_e and n_o, respectively.

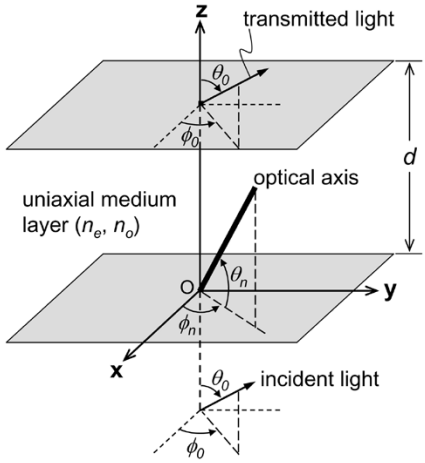

Fig. 2. Schematic view of an arbitrary light impinging on a uniaxial medium.

In general, the phase retardation of a uniaxial medium at oblique incidence can be expressed as [14]

$$\Gamma = (k_{e,z} - k_{o,z})d \tag{1}$$

where d is the layer thickness of the uniaxial medium, $k_{e,z}$ and $k_{o,z}$ are the z-axis components of wavevectors of extraordinary and ordinary waves, respectively. From Maxwell's equations, these two z-axis components of wavevectors $k_{e,z}$ and $k_{o,z}$ can be solved and given as (2) and (3) shown at the bottom of the page [15], with $\varepsilon_{xz} = \left(n_e^2 - n_o^2\right)\sin\theta_n\cos\theta_n\cos(\phi_n - \phi_0)$ and $\varepsilon_{zz} = n_o^2 + \left(n_e^2 - n_o^2\right)\sin^2\theta_n$. From (1) to (3), one can easily obtain the phase retardation Γ of a general uniaxial medium at an arbitrary incident angle, as shown in (4) at the bottom of the page. From (4), the phase retardation Γ is, in general, dependent on the optical axes orientation θ_n and ϕ_n as well as the beam incident direction θ_0 and ϕ_0.

In the uniaxial-film-compensated LCDs, both a- and c- films are commonly used. In these two special cases, (4) can be further simplified.

1) Phase Retardation of A-Film: For an a-film, its optical axis lies in the plane parallel to the film surface, i.e., $\theta_n = 0^\circ$

$$k_{e,z} = \frac{2\pi}{\lambda}\left[\frac{n_e n_o}{\varepsilon_{zz}}\sqrt{\varepsilon_{zz} - \left(1 - \frac{n_e^2 - n_o^2}{n_e^2}\cos^2\theta_n\sin^2(\phi_n - \phi_0)\right)\sin^2\theta_0} - \frac{\varepsilon_{xz}}{\varepsilon_{zz}}\sin\theta_0\right] \tag{2}$$

$$k_{o,z} = \frac{2\pi}{\lambda}\sqrt{n_o^2 - \sin^2\theta_0} \tag{3}$$

$$\Gamma = \frac{2\pi}{\lambda}d\left[\frac{n_e n_o}{\varepsilon_{zz}}\sqrt{\varepsilon_{zz} - \left(1 - \frac{n_e^2 - n_o^2}{n_e^2}\cos^2\theta_n\sin^2(\phi_n - \phi_0)\right)\sin^2\theta_0} - \frac{\varepsilon_{xz}}{\varepsilon_{zz}}\sin\theta_0 - \sqrt{n_o^2 - \sin^2\theta_0}\right] \tag{4}$$

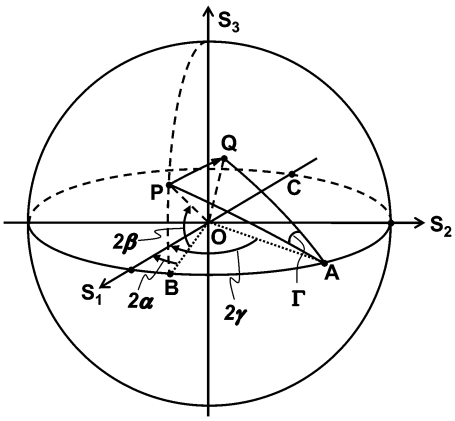

Fig. 3. Schematic diagram of Poincaré sphere representation and the effect of uniaxial medium on the polarization state change of a polarized incident light.

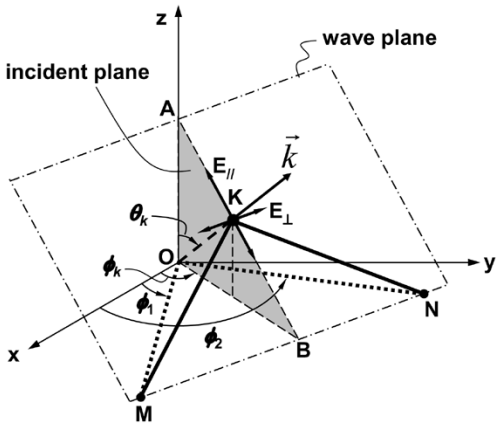

Fig. 4. Schematic view of the effective polarizer angle φ of two sheet polarizers on the wave plane of an oblique incident light.

Consequently, the phase retardation of the a-film at an arbitrary incident angle is given by (5), shown at the bottom of the page [14].

2) Phase Retardation of C-Film: In a c-film, its optical axis is perpendicular to the film surface, i.e., $\theta_n = 90°$. In this case, the phase retardation of the c-film at any oblique incidence is

$$\Gamma_c = \frac{2\pi}{\lambda} n_o d \left(\sqrt{1 - \frac{\sin^2\theta_0}{n_e^2}} - \sqrt{1 - \frac{\sin^2\theta_0}{n_o^2}} \right). \quad (6)$$

From (6), Γ_c is independent of the azimuthal angle ϕ_0 of the incident light. This is because the c-film's optical axis is perpendicular to its surface. Hence the optical properties of a c-film are axially symmetric around its optical axis.

C. Poincaré Sphere Representation

Poincaré sphere representation is an elegant geometrical means for solving problems involving the propagation of polarized light through birefringent and optically active media [13]. For an elliptically polarized light with long axis azimuthal angle α and ellipticity angle β, its polarization state can be represented by a point $\mathbf{P}$ on the Poincaré sphere with longitude 2α and latitude 2β, as is shown in Fig. 3. The radius of the sphere is one unit length. Here the long axis azimuthal angle γ of the elliptically polarized light is with respect to the x-axis. For a uniaxial film with its optical axis oriented at angle γ from the x-axis, it can be represented by point $\mathbf{A}$, which is located at longitude 2γ on the equator. Suppose the abovementioned elliptically polarized light (point $\mathbf{P}$) passes through the uniaxial film (point $\mathbf{A}$), the overall effect on Poincaré sphere is equivalent to rotate $\mathbf{AO}$ axis from point $\mathbf{P}$ to point $\mathbf{Q}$ by an angle Γ, which is determined by the phase retardation of the uniaxial film as expressed in (4). From spherical triangle definition, the spherical angle $\boldsymbol{PAQ}$ is equal to the rotation angle Γ. It should be pointed out that if the uniaxial film has a positive birefringence ($\Delta n = n_e - n_o > 0$), then the abovementioned rotation from point P to point Q is clockwise; otherwise, the rotation is counterclockwise if the uniaxial layer has a negative birefringence ($\Delta n < 0$).

For an a-film, its optical axis lies in the plane parallel to the film surface. When an observer views the LCD panel from different azimuthal and polar angles, the effective optical axis on the wave plane will change with the viewing direction. As a result, its position on the equator of Poincaré sphere will also change accordingly. On the other hand, a c-film's optical axis is perpendicular to the film surface. When an observer views the panel from different azimuthal and polar angles, the effective optical axis on the wave plane always forms 90° with respect to the horizontal reference. Therefore, its position on Poincaré sphere is always the intersection of equator and negative S_1 axis, which is denoted as point $\mathbf{C}$ in Fig. 3.

D. Light Leakage of Crossed Polarizers at Oblique View

Considering a pair of crossed sheet polarizers with their absorption axes perpendicular to each other, the effective angle between their respective absorption axes varies with different viewing directions. Fig. 4 shows the case when an oblique light traverses through two sheet polarizers. The polarizer's absorption axis $\mathbf{OM}$ makes an angle ϕ_1 with respect to the x-axis in the x-y plane while the analyzer's absorption axis $\mathbf{ON}$ is oriented at angle ϕ_2. The shadow triangle $\boldsymbol{OAB}$ in Fig. 4 denotes the plane of incidence. The light beam, denoted by the wave vector $\mathbf{OK}$, propagates at azimuthal angle ϕ_k and polar angle θ_k inside the sheet polarizer.

1) Effective Polarizer Angle on the Wave Plane: Although these two linear polarizers form an angle $(\phi_2 - \phi_1)$ in the x-y plane, their projections on the wave plane, however, form another angle $\angle\boldsymbol{MKN}$, as Fig. 4 plots. We call this angle $\angle\boldsymbol{MKN}$

$$\Gamma_a = \frac{2\pi}{\lambda} d \left[n_e \sqrt{1 - \frac{\sin^2\theta_0 \sin^2(\phi_n - \phi_0)}{n_e^2} - \frac{\sin^2\theta_0 \cos^2(\phi_n - \phi_0)}{n_o^2}} - n_o \sqrt{1 - \frac{\sin_2\theta_0}{n_o^2}} \right] \quad (5)$$

as the effective polarizer angle on the wave plane, which is expressed as φ hereafter. The extinction ratio of the crossed polarizers depends on this effective polarizer angle φ on the wave plane, rather than the absorption axes angle in the x-y plane.

Based on the dot product of vectors, the effective polarizer angle φ can be expressed as shown in (7) at the bottom of the page, where $\phi_k = \phi_0$ and $\theta_k = \sin^{-1}(\sin\theta_0/n_p)$. Here $n_p(\sim 1.5)$ is the average real refractive index of the sheet polarizer, and ϕ_0 and θ_0 are the azimuthal and incident angles of the incident light measured in air, respectively. In WVA LCDs, the absorption axes of polarizer and analyzer are usually perpendicular to each other. If we set $\phi_1 = 45°$ and $\phi_2 = -45°$, then the effective polarizer angle φ can be rewritten as shown in (8) at the bottom of the page. As a quick verification, under normal view ($\theta_k = 0°$), the effective polarizer angle φ equals to 90°, which is identical to the absorption axes angle in the x-y plane, i.e., $\phi_2 - \phi_1 = 90°$.

To find the tendency of φ when the azimuthal angle $\phi_0(=\phi_k)$ changes, we take the first-order derivative of φ with respect to ϕ_k and obtain

$$\frac{\partial\varphi}{\partial\phi_k} = -\frac{\sin^2\theta_k\cos\theta_k\sin 2\phi_k}{\cos^2\theta_k + \frac{1}{4}\sin^4\theta_k\cos^2 2\phi_k}. \tag{9}$$

Apparently, when $\phi_k = \phi_0 = 0°$, 90°, 180°, and 270°, the effective polarizer angle φ reaches extrema. The second-order derivative

$$\frac{\partial^2\varphi}{\partial\phi_k^2} = -\frac{2\sin^2\theta_k\cos\theta_k\cos 2\phi_k}{\cos^2\theta_k + \frac{1}{4}\sin^4\theta_k\cos^2 2\phi_k} - \frac{\sin^6\theta_k\cos\theta_k\sin^2 2\phi_k\cos 2\phi_k}{\left(\cos^2\theta_k + \frac{1}{4}\sin^4\theta_k\cos^2 2\phi_k\right)^2} \tag{10}$$

further reveals that φ reaches maxima at $\phi_k = \phi_0 = 0°$ and 180° and minima at $\phi_k = \phi_0 = 90°$ and 270°. By substituting $\phi_k = \phi_0 = 270°$ into (8), we derive the effective polarizer angle φ at the lower bisector viewing position [16]:

$$\varphi = \cos^{-1}\left(\frac{\frac{\sin^2\theta_o}{n_p^2}}{2 - \frac{\sin^2\theta_0}{n_p^2}}\right) \tag{11}$$

where θ_0 is the incident angle measured in air and n_p is the average real refractive index of the sheet polarizer. This equation will be frequently referred in Sections III and IV.

Fig. 5(a) plots the dependence of effective polarizer angle φ on viewing the polar angle θ_0 and azimuthal angle ϕ_0 as calculated from (8). During calculations, the average real refractive index of the sheet polarizer is taken to be $n_p = 1.5$. From Fig. 5(a), at off-axis viewing directions, the effective polarizer angle φ deviates from 90°. Especially in all the bisector viewing directions, i.e., $\phi_0 = 0°$, 90°, 180°, and 270°, the effective polarizer angle φ deviates the farthest from 90° and reaches either

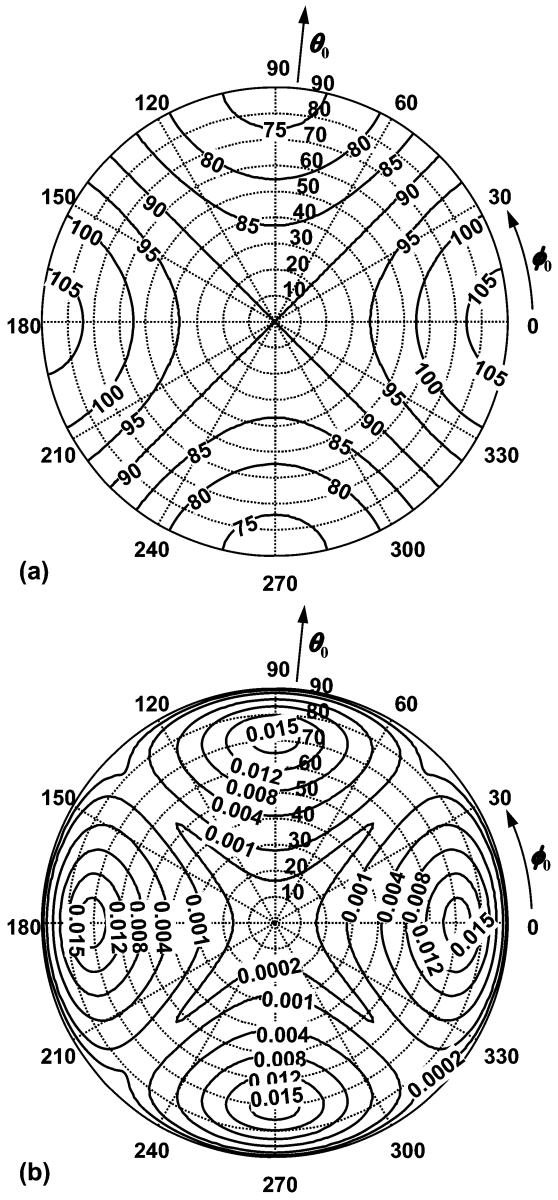

Fig. 5. Dependence of (a) effective polarizer angle φ and (b) dark state light leakage of crossed sheet polarizers on the viewing azimuthal angle ϕ_0 and polar angle θ_0. The absorption axes of the crossed sheet polarizers are set at 45° and $-45°$, respectively, and the wavelength of incident light is $\lambda = 550$ nm.

$$\varphi = \cos^{-1}\left[\frac{\cos(\phi_2-\phi_1) - \sin^2\theta_k\cos(\phi_1-\phi_k)\cos(\phi_2-\phi_k)}{\sqrt{1-\sin^2\theta_k\cos^2(\phi_1-\phi_k)}\sqrt{1-\sin^2\theta_k\cos^2(\phi_2-\phi_k)}}\right] \tag{7}$$

$$\varphi = \cos^{-1}\left[\frac{-\sin^2\theta_k\cos\left(\frac{\pi}{4}-\phi_k\right)\cos\left(\frac{\pi}{4}+\phi_k\right)}{\sqrt{1-\sin^2\theta_k\cos^2\left(\frac{\pi}{4}-\phi_k\right)}\sqrt{1-\sin^2\theta_k\cos^2\left(\frac{\pi}{4}+\phi_k\right)}}\right] \tag{8}$$

maxima or minima. By contrast, in all on-axis viewing directions, i.e., $\phi_0 = 45°$, 135°, 225°, and 315°, the effective polarizer angle φ equals to 90°, same as the normal view.

The effective polarizer angle deviating from 90° at off-axis viewing directions causes dark-state light leakage which, in turn, degrades the device contrast ratio. As a typical example, Fig. 5(b) shows the dark-state light leakage of crossed polarizers calculated by the extended Jones matrix method [15], [17]. In the calculation, both sheet polarizers are treated as anisotropic uniaxial media with complex refractive indices $n_e = 1.5 + j0.0022$ and $n_o = 1.5 + j0.000\,032$. As Fig. 5(b) shows, the light leakage reaches maxima at the bisector viewing directions, i.e., $\phi_0 = 0°$, 90°, 180°, and 270°.

2) Crossed Polarizers on Poincaré Sphere: The dark state light leakage of crossed polarizers can also be well explained on the Poincaré sphere, as shown in Fig. 6(a) and (b). To facilitate the representation on Poincaré sphere, we still set $\phi_1 = 45°$ and $\phi_2 = -45°$, keeping the absorption axes of these two sheet polarizers perpendicular to each other in the x-y plane. Fig. 6(a) represents the viewing from normal direction, while Fig. 6(b) stands for an oblique view from the lower bisector, i.e., $\phi_0 = 270°$. In both figures, points $\mathbf{P}$ and $\mathbf{A}$ represent the effective absorption axis positions of polarizer and analyzer on the wave plane, respectively. The polarization state of the linearly polarized light after the polarizer, which is denoted by point $\mathbf{T}$, is always orthogonal to the absorption axis direction of the polarizer on the wave plane. Therefore, on the Poincaré sphere, point $\mathbf{T}$ and point $\mathbf{P}$ are always located at the opposite sides along the diameter of the sphere.

As shown in Fig. 6(a), under normal view the absorption axes of polarizer (point $\mathbf{P}$) and analyzer (point $\mathbf{A}$) are located at 90° and $-90°$ on the equator of Poincaré sphere, respectively. Point $\mathbf{T}$, the polarization state of the linearly polarized light after the polarizer, overlaps exactly with point $\mathbf{A}$, the absorption axis of the analyzer, resulting in complete light absorption and no light leakage from normal viewing direction.

However, under oblique view from the lower bisector direction $\phi_0 = 270°$, the effective absorption axis positions of both polarizer and analyzer move toward the horizontal reference. Accordingly, from the lower bisector viewing direction $\phi_0 = 270°$, the effective polarizer angle φ becomes less than 90° as illustrated in Fig. 5(a). As a result, on the Poincaré sphere, points $\mathbf{P}$ and $\mathbf{A}$ are no longer located on the S_2 axis. Instead, point $\mathbf{P}$ is located between S_1 and S_2 axes, while point $\mathbf{A}$ is located between S_1 and negative S_2 axes, as Fig. 6(b) shows. Moreover, point $\mathbf{P}$ is symmetric to point $\mathbf{A}$ about S_1 axis, and angle $\angle \boldsymbol{POA}$ is twice the effective polarizer angle φ, i.e., $\angle \boldsymbol{POA} = 2\varphi$. Meanwhile, point $\mathbf{T}$, representing the polarization state of light after the polarizer, is on the other end of the diameter passing through point $\mathbf{P}$. Therefore, point $\mathbf{T}$ also deviates from the negative S_2 axis and is located symmetrically to point $\mathbf{A}$ with respect to the negative S_2 axis. Because point $\mathbf{T}$ no longer overlaps with point $\mathbf{A}$, light leakage occurs from the bisector viewing direction of the crossed polarizers.

It is easy to figure out the relationship $\angle \boldsymbol{TOA} = \pi - 2\varphi$ from Fig. 6(b). The larger the angle $\angle \boldsymbol{TOA}$ is, the more severe the light leakage becomes. Since the effective polarizer angle φ deviates the farthest from 90° at all bisector viewing positions, the light leakage at bisectors is the severest, as depicted in Fig. 5(b). If we can suppress the light leakage for all the bisector positions, the viewing angle of the LCD will be significantly enhanced. Thus, the goal of WVA LCDs, which incorporate compensation films into the panel design, is to move point $\mathbf{T}$ to point $\mathbf{A}$ for minimizing the light leakage from the analyzer. The introduced compensation film should improve the off-axis viewing performance but not affect the on-axis viewing performance.

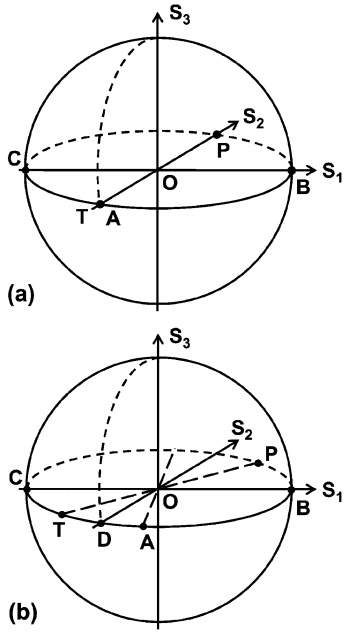

Fig. 6. Demonstration of crossed polarizers on Poincaré sphere under (a) normal view and (b) oblique view at the lower bisector position $\phi_0 = 270°$. Here the absorption axes of polarizer and analyzer are set at $\phi_1 = 45°$ and $\phi_2 = -45°$, respectively.

In Sections III and IV, we will analyze the compensation schemes of various uniaxial-film-compensated WVA LCDs and derive analytical solutions for each scheme.

III. Compensation Schemes for LCD With Initially Homogeneous Alignment

In the WVA LCDs with initially homogeneous alignment, such as IPS and FFS modes, let us assume the stripe electrodes are in the bottom substrate and the electric fields are in the horizontal direction. As the applied voltage exceeds the threshold voltage, i.e., $V > V_{th}$, the LC directors are gradually twisted from the anchored bottom boundary layer to the middle and then twisted back from the middle to the top (unaffected) boundary layer. Although FFS mode can achieve a higher optical efficiency than IPS, their viewing angle performances are quite similar. For benchmarking, Fig. 7 plots the calculated iso-contrast contours of an uncompensated IPS-LCD. In the calculation throughout this section, unless otherwise specified, we assume that at bright-state the middle layer LC directors are twisted 65° with respect to both boundary layers. Other parameters employed in simulations are listed in Table II.

From Fig. 7, without compensation films the IPS viewing angle at bisectors $\phi_0 = 0°$, 90°, 180°, and 270° are relatively poor. At bisectors, the 10:1 contrast ratio only extends to $\sim 70°$

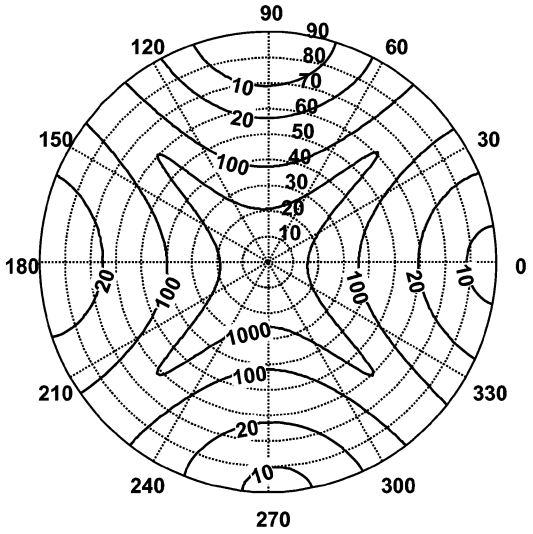

Fig. 7. Iso-contrast contour of an uncompensated IPS-LCD at $\lambda = 550$ nm.

TABLE II
PARAMETERS USED IN SIMULATING THE IPS-LCD VIEWING ANGLE PERFORMANCE

Parameters	Description	Values
d_{LC}	Cell gap	4 μm
$\theta_{pretilt}$	Surface tilt angle	1°
$n_{LC,e}$	n_e of LC material	1.5649
$n_{LC,o}$	n_o of LC material	1.4793
$n_{p,e}$	n_e of sheet polarizer (complex)	1.5+j0.0022
$n_{p,o}$	n_o of sheet polarizer (complex)	1.5+j0.000032
$n_{c+,e}$	n_e of positive c-film	1.5110
$n_{c+,o}$	n_o of positive c-film	1.5095
$n_{c-,e}$	n_e of negative c-film	1.5095
$n_{c-,o}$	n_o of negative c-film	1.5110
$n_{a+,e}$	n_e of positive a-film	1.5110
$n_{a+,o}$	n_o of positive a-film	1.5095
$n_{a-,e}$	n_e of negative a-film	1.5095
$n_{a-,o}$	n_o of negative a-film	1.5110
ϕ_1	Absorption axis of polarizer	45°
ϕ_2	Absorption axis of analyzer	−45° (or 135°)
λ	Wavelength of incident light	550 nm

polar angle. This is due to the large dark-state light leakage at these bisector positions, as depicted in Fig. 5(b).

In the following, we use IPS-LCD as an example to demonstrate three compensation schemes and provide each scheme a comprehensive analytical solution. These compensation schemes are equally applicable to FFS-LCDs.

A. One Positive A-Film and One Positive C-Film

Fig. 8(a) shows the device configuration of an IPS-LCD using one positive a-film and one positive c-film for phase compensation. This compensation scheme was first proposed by Chen [7] and later confirmed by Anderson [8]. As shown in Fig. 8(a), a positive c-film and a positive a-film are sandwiched between the analyzer and the homogeneous LC layer. More specifically, the positive a-film, whose optical axis is oriented parallel to the absorption axis of the polarizer, is adjacent to the analyzer. Fig. 8(b) explains the compensation principle on

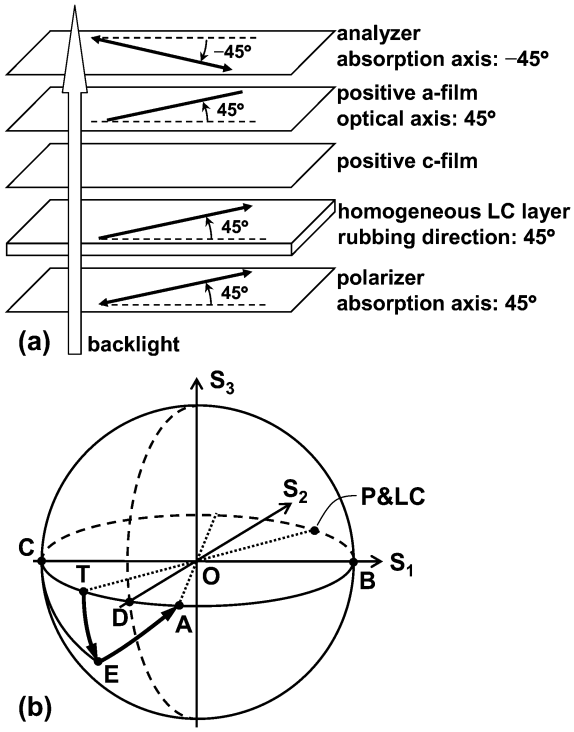

Fig. 8. (a) Device structure and (b) compensation principle of an IPS-LCD with compensation of a positive a-film and a positive c-film.

Poincaré sphere when the observer views the panel from an oblique angle at the lower bisector position $\phi_0 = 270°$.

The detailed compensation mechanism is explained as Fig. 8(b) shows. When the unpolarized light from backlight unit traverses the polarizer (point $\mathbf{P}$), it becomes linearly polarized, and its polarization state is located at point $\mathbf{T}$, which deviates from the absorption axis of the analyzer (point $\mathbf{A}$). When such a linearly polarized light (point $\mathbf{T}$) passes through the homogenous LC layer, whose position on the Poincaré sphere overlaps with point $\mathbf{P}$, the linear polarization state still keeps the same (point $\mathbf{T}$). Then, the linearly polarized light (point $\mathbf{T}$) successively passes through the positive c-film and the positive a-film, whose effective optical axis positions on the Poincaré sphere are point $\mathbf{C}$ and point $\mathbf{P}$, respectively. When the linearly polarized light (point $\mathbf{T}$) passes through the positive c-film, its polarization state is rotated from point $\mathbf{T}$ to point $\mathbf{E}$ clockwise around the $\mathbf{CO}$ axis. This intermediate polarization state (point $\mathbf{E}$), in general, is elliptical. By properly choosing the phase retardation values of the positive a- and c- films, we can always fulfill the following goal: when the elliptically polarized light (point $\mathbf{E}$) passes through the positive a-film, the polarization state can be rotated clockwise around the $\mathbf{PO}$ axis so that point $\mathbf{E}$ is moved to point $\mathbf{A}$. As a result, at $V = 0$ the light is completely absorbed by the analyzer (point $\mathbf{A}$), leading to a good dark state even viewed from an oblique angle at the bisectors.

To reach the abovementioned goal, we can easily determine from Fig. 8(b) that the following two requirements must be satisfied: (1) the arc $\overline{\boldsymbol{TE}}$ should equal to the arc $\overline{\boldsymbol{TA}}$, and (2) the arc $\overline{\boldsymbol{TC}}$ should equal to the arc $\overline{\boldsymbol{EC}}$. Besides, from Fig. 8(b) we can also obtain $\angle \boldsymbol{POB} = \angle \boldsymbol{AOB} = \varphi$, $\overline{\boldsymbol{TA}} = \pi - 2\varphi$,

and $\overline{TC} = \varphi$. Based on spherical trigonometry, we can find the following relationships from the spherical triangles $\boldsymbol{CTE}$ and $\boldsymbol{TEA}$:

$$\angle TCE = 2\sin^{-1}(\mathrm{ctg}\varphi), \tag{12a}$$

$$\angle CTE = \cos^{-1}(\mathrm{ctg}^2\varphi), \tag{12b}$$

$$\angle ATE = \pi - \angle CTE \tag{12c}$$

where φ, determined by (11), is the effective polarizer angle on the wave plane from the lower bisector viewing position $\phi_0 = 270°$.

Since the required positive c-film's phase retardation Γ_{c+} equals to the spherical angle $\angle\boldsymbol{TCE}$, thus from (6) and (12a) the required positive c-film's thickness d_{c+} can be derived as:

$$d_{c+} = \lambda \frac{\frac{\sin^{-1}(\mathrm{ctg}\varphi)}{\pi}}{n_{c+,o}\left(\sqrt{1-\frac{\sin^2\theta_0}{n_{c+,e}^2}} - \sqrt{1-\frac{\sin^2\theta_0}{n_{c+,o}^2}}\right)}. \tag{13}$$

On the other hand, the required positive a-film's phase retardation Γ_{a+} equals to the spherical angle $\angle\boldsymbol{ATE}$. Thus from (5), (12b) and (12c) we can derive the required positive a-film's thickness d_{a+} as:

$$d_{a+} = \lambda \frac{\frac{1}{2} - \frac{\cos^{-1}(\mathrm{ctg}^2\varphi)}{2\pi}}{n_{a+,e}\sqrt{1-\frac{\sin^2\theta_0}{2n_{a+,e}} - \frac{\sin^2\theta_0}{2n_{a+,o}}} - n_{a+,o}\sqrt{1-\frac{\sin^2\theta_0}{n_{a+,o}^2}}}. \tag{14}$$

In the derivation of (14), we substitute $\phi_n = 45°$ and $\phi_0 = 270°$ into (5) because the positive a-film's optical axis is oriented at 45° direction, as Fig. 8(a) shows, and the viewing direction is at $\phi_0 = 270°$ azimuthal angle.

As we can see from (11), (13), and (14), the required film thickness depends on the incident angle θ_0, film's refractive indices $n_{c+,e}$, $n_{c+,o}$, $n_{a+,e}$, and $n_{a+,o}$, and polarizer's average real refractive index n_p. Therefore, once we know both films' and polarizer's refractive indices, and the intended viewing angle (i.e., incident angle), we can determine the required film thickness from (11), (13), and (14). For instance, if we set $\theta_0 = 70°$ as the intended viewing angle where we would like to optimize our LCD designs, and use the parameters listed in Table II, then we can calculate the required film thicknesses from (13) and (14). Results are $d_{c+} = 60.09\ \mu$m and $d_{a+} = 92.59\ \mu$m. Based on these film thicknesses, Fig. 9 depicts the calculated iso-contrast contour of an IPS-LCD with one positive a-film and one positive c-film for phase compensation. Comparing Fig. 9 with Fig. 7, we can clearly see that the viewing angle performance at off-axis viewing directions, especially the bisector positions $\phi_0 = 0°$, 90°, 180°, and 270°, is dramatically improved. Meanwhile, the contrast ratios at on-axis viewing directions $\phi_0 = 45°$, 135°, 225°, and 315° remain unchanged.

This compensation scheme can also be modified by exchanging the positions of the positive c-film and a-film, as shown in Fig. 10(a). Different from Fig. 8(a), now the positive a-film is adjacent to the LC layer and its optical axis is parallel to the absorption axis of the analyzer. The compensation principle is demonstrated in Fig. 10(b). When the linearly

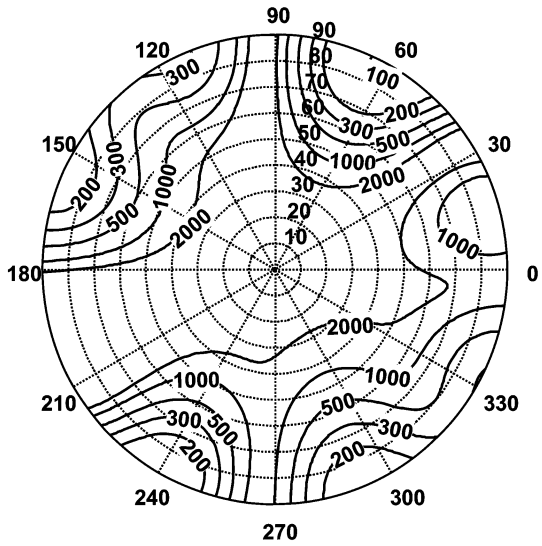

Fig. 9. Iso-contrast contour of an IPS-LCD with a positive a-film ($d_{a+} = 92.59\ \mu$m) and a positive c-film ($d_{c+} = 60.09\ \mu$m) under $\lambda = 550$ nm.

polarized light (point $\mathbf{T}$) passes through the positive a-film, the polarization state is rotated clockwise around the $\mathbf{AO}$ axis so that point $\mathbf{T}$ is moved to point $\mathbf{E}$. Now the intermediate state (point $\mathbf{E}$) is located on the upper hemisphere. The role of the positive c-film is to rotate point $\mathbf{E}$ to point $\mathbf{A}$ clockwise around the $\mathbf{CO}$ axis. Although the process of polarization state change is different, the required film thickness values, however, are still identical to those of the previous case as determined by (13) and (14). Its viewing angle is similar to Fig. 9. To avoid redundancy, the iso-contrast contour plot is not shown here.

Actually, this compensation scheme can be further modified by replacing both positive a-film and positive c-film with a negative a-film and a negative c-film. In addition, the positions of the negative a-film and c-film are also exchangeable, just like the configurations shown in Figs. 8(a) and 10(a). Still, the compensation mechanisms are similar to those with positive a- and c- films as Figs. 8(b) and 10(b) depict. However, the rotation on the Poincaré sphere becomes counterclockwise in the case of negative uniaxial films. The required film thickness can still be determined by (13) and (14) except: (1) substituting λ with $-\lambda$ due to negative phase retardation of the negative uniaxial films, and (2) replacing the positive films' refractive indices $n_{c+,e}$, $n_{c+,o}$, $n_{a+,e}$, and $n_{a+,o}$ with the corresponding negative films' refractive indices $n_{c-,e}$, $n_{c-,o}$, $n_{a-,e}$, and $n_{a-,o}$. The resultant viewing angle performance is still similar to Fig. 9, which is not repeated here to avoid redundancy. In summary, the compensation schemes with a- and c- films have four different configurations.

Although the contrast ratio of this compensation scheme exceeds 100:1 at any viewing directions, we still notice from Fig. 9 that the viewing angle is not very symmetric. This is because the intermediate state (point $\mathbf{E}$) is not located on the great circle passing through S_2 and S_3 axes, as shown in Figs. 8(b) and 10(b). To get a more symmetric viewing angle, we need to make the intermediate state located on the great circle which passes through S_2 and S_3 axes and bisects the arc $\overline{\boldsymbol{TA}}$, as will be discussed in Sections III-B and C.

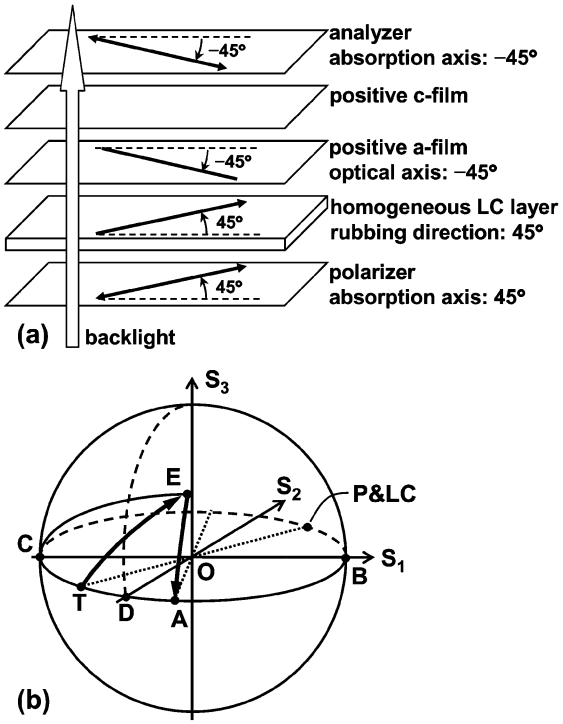

Fig. 10. (a) Device structure and (b) compensation principle of another IPS-LCD using one positive a-film and one positive c-film.

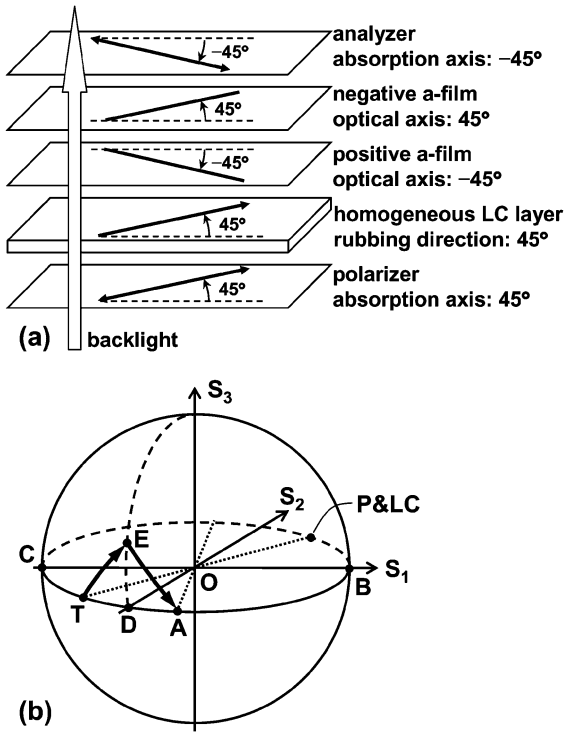

Fig. 11. (a) Device structure and (b) compensation principle of an IPS-LCD with compensation of one positive a-film and one negative a-film.

B. One Positive A-Film and One Negative A-Film

Fig. 11(a) shows the device configuration of an IPS-LCD with one positive a-film and one negative a-film compensation. This mode was previously reported by our group [18], [19]. As shown in the figure, a positive a-film and a negative a-film are sandwiched between the LC layer and the analyzer, with the positive a-film adjacent to the LC layer. More specifically, the optical axis of the positive a-film is parallel to the absorption axis of the analyzer, while the optical axis of the negative a-film is parallel to the absorption axis of the polarizer. Fig. 11(b) explains the compensation principle on Poincaré sphere when the observer views the panel from an oblique angle at the lower bisector position, i.e., $\phi_0 = 270°$.

The detailed compensation mechanism is explained as Fig. 11(b) demonstrates. When the unpolarized light from backlight penetrates the polarizer (point $\mathbf{P}$), it becomes linearly polarized and its polarization state is located at point $\mathbf{T}$, which deviates from the absorption axis of the analyzer (point $\mathbf{A}$). When such a linearly polarized light (point $\mathbf{T}$) passes through the homogenous LC layer, whose position on the Poincaré sphere overlaps with point $\mathbf{P}$, the linear polarization state remains the same (point $\mathbf{T}$). Then, the linearly polarized light (point $\mathbf{T}$) successively passes through the positive a-film and the negative a-film, whose positions on the Poincaré sphere are point $\mathbf{A}$ and point $\mathbf{P}$, respectively. When the linearly polarized light (point $\mathbf{T}$) passes through the positive a-film, its polarization state is rotated clockwise from point $\mathbf{T}$ to point $\mathbf{E}$ around the $\mathbf{AO}$ axis. This intermediate polarization state (point $\mathbf{E}$), in general, is an elliptical polarization state. By properly choosing the phase retardation values of both positive a-film and negative a-film, we should be able to rotate point $\mathbf{E}$ to point $\mathbf{A}$ counterclockwise around the $\mathbf{PO}$ axis. As a result, in the voltage-off state the light is completely absorbed by the analyzer (point $\mathbf{A}$) and a very good dark state is achieved even viewed from an oblique angle at the bisector positions.

To reach this goal, we can easily determine from Fig. 11(b) that the following two requirements must be satisfied: (1) the arc $\overline{\boldsymbol{EA}}$ should equal to the arc $\overline{\boldsymbol{TA}}$; and (2) the arc $\overline{\boldsymbol{TA}}$ should equal to the arc $\overline{\boldsymbol{TE}}$. In other words, the spherical triangle $\boldsymbol{ETA}$ should be an equilateral spherical triangle. In addition, we can also obtain $\angle\boldsymbol{POB} = \angle\boldsymbol{AOB} = \varphi$ and $\overline{\boldsymbol{TA}} = \pi - 2\varphi$ from the Poincaré sphere. Based on the spherical trigonometry, we derive the following relationship from the equilateral spherical triangle $\boldsymbol{ETA}$:

$$\angle ETA \equiv \angle EAT = \cos^{-1}(-\mathrm{ctg}\varphi \cdot \mathrm{ctg}2\varphi), \qquad (15)$$

where φ, determined by (11), is the effective polarizer angle on the wave plane from the lower bisector viewing position, i.e., $\phi_0 = 270°$.

Since the required positive a-film's phase retardation Γ_{a+} equals to the spherical angle $\angle\boldsymbol{EAT}$, thus from (5) and (15) the required positive a-film's thickness d_{a+} can be expressed as:

$$d_{a+} = \lambda \frac{\frac{\cos^{-1}(-\mathrm{ctg}\varphi \cdot \mathrm{ctg}2\varphi)}{2\pi}}{n_{a+,e}\sqrt{1 - \frac{\sin^2\theta_0}{2n_{a+,e}^2} - \frac{\sin^2\theta_0}{2n_{a+,o}^2}} - n_{a+,o}\sqrt{1 - \frac{\sin^2\theta_o}{n_{a+,o}^2}}}. \qquad (16)$$

In the derivation of (16), we substitute $\phi_n = -45°$ and $\phi_0 = 270°$ into (5) because the positive a-film's optical axis is oriented at $-45°$ direction, as Fig. 11(a) shows, and the viewing direction is from $\phi_0 = 270°$ azimuthal angle.

Similarly, the negative a-film's phase retardation Γ_{a-} is equal to the negative spherical angle $\angle\boldsymbol{ETA}$, *i.e.*, $\Gamma_{a-} = -\angle\boldsymbol{ETA}$.

Here the minus sign denotes that the phase retardation of the negative a-film is negative and the rotation around $\mathbf{PO}$ axis from point $\mathbf{E}$ to point $\mathbf{A}$ is counterclockwise. Thus from (5) and (15) we can obtain the negative a-film's thickness d_{a-} as:

$$d_{a-} = -\lambda \times \frac{\frac{\cos^{-1}(-\mathrm{ctg}\varphi \cdot \mathrm{ctg}2\varphi)}{2\pi}}{n_{a-,e}\sqrt{1-\frac{\sin^2\theta_0}{2n_{a-,e}^2}-\frac{\sin^2\theta_0}{2n_{a-,o}^2}}-n_{a-,o}\sqrt{1-\frac{\sin^2\theta_o}{n_{a-,o}^2}}}. \quad (17)$$

In the derivation of (17), we substitute $\phi_n = 45°$ and $\phi_0 = 270°$ into (5) because the negative a-film's optical axis is oriented at 45° direction, as Fig. 11(a) shows, and the viewing direction is from $\phi_0 = 270°$ azimuthal angle.

From (11), (16), and (17), the required film thicknesses depend on the incident angle θ_0, film's refractive indices $n_{a+,e}$, $n_{a+,o}$, $n_{a-,e}$, and $n_{a-,o}$, and polarizer's average real refractive index n_p. Therefore, once we know both films' and polarizer's refractive indices as well as the intended viewing angle for LCD optimization, we can determine the required film thickness from (11), (16), and (17). By using the parameters listed in Table II and choosing $\theta_0 = 70°$, the required film thicknesses as calculated from (16) and (17) are $d_{a+} = 61.38\ \mu$m and $d_{a-} = 61.37\ \mu$m. Based on these film thicknesses, Fig. 12 plots the calculated iso-contrast contour of the IPS-LCD with one positive a-film and one negative a-film. Comparing Fig. 12 with Fig. 7, we see clearly that the viewing characteristic at off-axis directions, especially the bisector positions $\phi_0 = 0°$, 90°, 180°, and 270°, is dramatically improved. In the mean time, the contrast ratios along the horizontal and vertical axes ($\phi_0 = 45°$, 135°, 225°, and 315°) remain unchanged.

It deserves a special mention that in the design shown in Fig. 11(a), the positions of the positive a-film and the negative a-film are exchangeable. We have gone through the simulation and found that the required film thicknesses remain the same. The Poincaré representation is still similar except that the intermediate polarization state (point $\mathbf{E}$) is on the lower hemisphere. The required film thickness d_{a+} and d_{a-} are still the same as obtained in (16) and (17). Finally, the viewing angle performance is almost identical to those shown in Fig. 12.

As shown in Fig. 12, the contrast ratio exceeds 200:1 from all viewing directions. This viewing angle is more symmetric than that shown in Fig. 9 using one positive a-film and one positive c-film for compensation. This is due to the fact that in this compensation scheme the intermediate state (point $\mathbf{E}$) is located on the great circle which passes through S_2 and S_3 axes and bisects the arc $\overline{TA}$. Another beauty of this compensation scheme is that it does not require any c-film or biaxial film; only uniaxial a-films are required. Since a-film has a lower cost than c-film and biaxial film, this compensation scheme has potentially low cost while keeping excellent viewing characteristics.

C. Two Positive A-Films and One Positive C-Film

Fig. 13(a) shows the device configuration of the IPS-LCD with two positive a-films and one positive c-film. As shown in the figure, the positive c-film is sandwiched between two positive a-films, and all of these three uniaxial films are further laminated between the homogeneous LC layer and the analyzer.

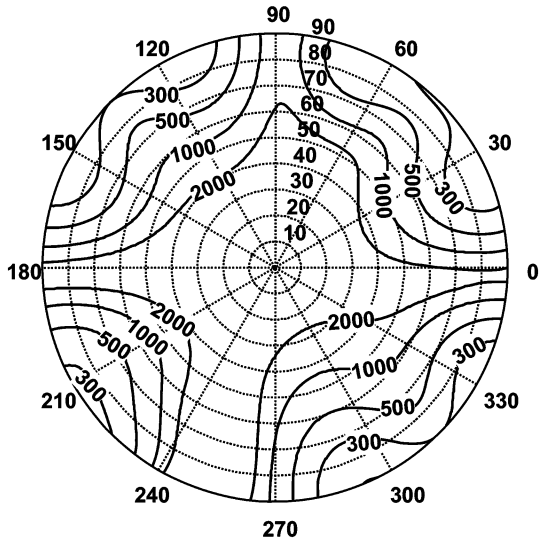

Fig. 12. Iso-contrast contour of the IPS-LCD with a positive a-film ($d_a = 61.38\ \mu$m) and a negative a-film ($d_a - = 61.37\ \mu$m) under $\lambda = 550$ nm.

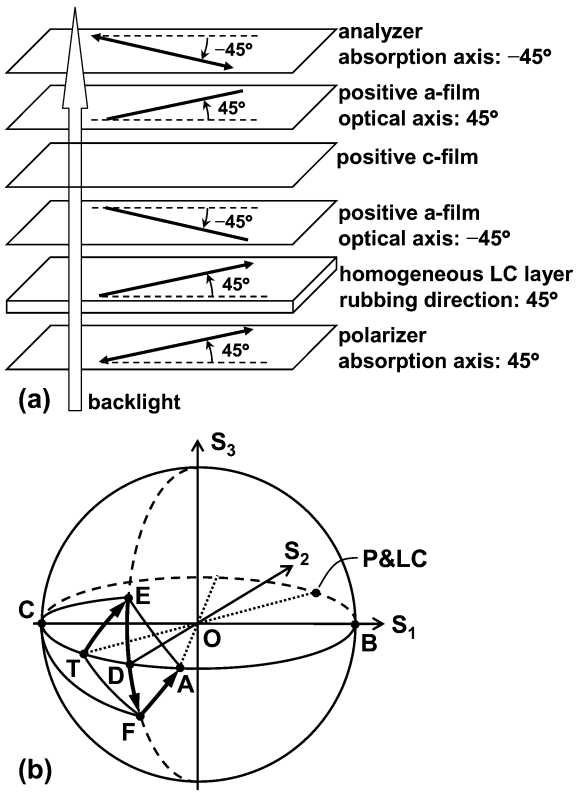

Fig. 13. (a) Structure and (b) compensation principle of IPS-LCD with compensation of two positive a-films and one positive c-film.

More specifically, the optical axis of the bottom positive a-film is parallel to the absorption axis of the analyzer, while the optical axis of the top positive a-film is parallel to the absorption axis of the polarizer. Fig. 13(b) explains the compensation principle on Poincaré sphere when the observer views the panel from an oblique angle at the lower bisector position $\phi_0 = 270°$.

The detailed compensation mechanism is explained as Fig. 13(b) depicts. When the unpolarized light from backlight unit penetrates the polarizer (point $\mathbf{P}$), it becomes linearly

polarized, and its polarization state is located at point $\mathbf{T}$, which deviates from the absorption axis of the analyzer (point $\mathbf{A}$). When such a linearly polarized light (point $\mathbf{T}$) passes through the homogenous LC layer, whose position on the Poincaré sphere overlaps with point $\mathbf{P}$, the linear polarization state is kept the same (point $\mathbf{T}$). Then, the linearly polarized light (point $\mathbf{T}$) successively passes through the bottom positive a-film, the positive c-film, and the top positive a-film, whose positions on the Poincaré sphere are points $\mathbf{A}$, $\mathbf{C}$, and $\mathbf{P}$, respectively. When the linearly polarized light (point $\mathbf{T}$) passes through the bottom positive a-film, its polarization state is clockwise rotated from point $\mathbf{T}$ to point $\mathbf{E}$ around the $\mathbf{AO}$ axis. This first intermediate polarization state (point $\mathbf{E}$), in general, is elliptical. When this elliptically polarized light traverses the positive c-film, its polarization state is clockwise rotated from point $\mathbf{E}$ to point $\mathbf{F}$ around the $\mathbf{CO}$ axis. This is the second intermediate polarization state. Again, the second intermediate state is also elliptical. As mentioned in Section III-A, to get a symmetric viewing characteristic, it is preferable to have the intermediate states (points $\mathbf{E}$ and $\mathbf{F}$) located on the great circle passing through S_2 and S_3 axes. In addition, it is also preferable to keep points $\mathbf{E}$ and $\mathbf{F}$ symmetric about the equator plane.

By properly choosing the phase retardation values of these two positive a-films and the positive c-film, we can always rotate point $\mathbf{F}$ to $\mathbf{A}$ clockwise around the $\mathbf{PO}$ axis. As a result, in the voltage-off state the light is completely absorbed by the analyzer (point $\mathbf{A}$) and a good dark state is achieved even viewed from an oblique angle at the bisector positions.

To derive the required film thicknesses, from Fig. 13(b) we find that the following three requirements must be satisfied: 1) the arcs $\overline{\boldsymbol{EA}}$, $\overline{\boldsymbol{ET}}$, $\overline{\boldsymbol{TA}}$, $\overline{\boldsymbol{TF}}$, and $\overline{\boldsymbol{AF}}$ all should be equal to each other; (2) the arc $\overline{\boldsymbol{CE}}$ should be equal to the arc $\overline{\boldsymbol{CF}}$; and 3) the arc $\overline{\boldsymbol{EF}}$ should be perpendicular to the equator. Therefore, both spherical triangles $\boldsymbol{ETA}$ and $\boldsymbol{FTA}$ should be equilateral spherical triangles. Besides, we also obtain $\angle\boldsymbol{POB} = \angle\boldsymbol{AOB} = \varphi$ and $\overline{\boldsymbol{TA}} = \pi - 2\varphi$ on the Poincaré sphere. Based on spherical trigonometry, we can derive the following relationships from the spherical angle $\boldsymbol{CEF}$ and the equilateral spherical triangles $\boldsymbol{ETA}$ and $\boldsymbol{FTA}$:

$$\angle EAT \equiv \angle ATF = \cos^{-1}(-\mathrm{ctg}\varphi \cdot \mathrm{ctg}2\varphi) \tag{18a}$$

$$\overline{ED} \equiv \overline{FD} = \cos^{-1}\left(\frac{-\cos 2\varphi}{\sin\varphi}\right) \tag{18b}$$

$$\angle ECF = 2\overline{ED} = 2\cos^{-1}\left(\frac{-\cos 2\varphi}{\sin\varphi}\right) \tag{18c}$$

where φ, determined by (11), is the effective polarizer angle on the wave plane from the lower bisector viewing position $\phi_0 = 270^\circ$.

Since the spherical angle $\angle\boldsymbol{EAT}$ is equal to the spherical angle $\angle\boldsymbol{ATF}$, the required phase retardation values for both bottom and top positive a-films also should be equal to each other. Thus from (5) and (18a), the required thickness d_{a+} for both positive a-films can be expressed as

$$d_{a+} = \lambda \frac{\frac{\cos^{-1}(-\mathrm{ctg}\varphi \cdot ctg2\varphi)}{2\pi}}{n_{a+,e}\sqrt{1 - \frac{\sin^2\theta_0}{2n_{a+,e}^2} - \frac{\sin^2\theta_0}{2n_{a+,o}^2}} - n_{a+,o}\sqrt{1 - \frac{\sin^2\theta_0}{n_{a+,o}^2}}}. \tag{19}$$

In the derivation of the above equation, we substitute $\phi_n = \pm 45^\circ$ and $\phi_0 = 270^\circ$ into (5) because the positive a-films' optical axes are oriented at $\phi_n = -45^\circ$ and $\phi_n = 45^\circ$, respectively, as Fig. 13(a) shows, and the viewing direction is at $\phi_0 = 270^\circ$ azimuthal angle.

On the other hand, the required positive c-film's phase retardation Γ_{c+} equals to the spherical angle $\angle\boldsymbol{ECF}$. Thus from (5) and (18c) we derive the positive c-film's thickness d_{c+} as

$$d_{c+} = \lambda \frac{\frac{\cos^{-1}\left(\frac{-\cos 2\varphi}{\sin\varphi}\right)}{\pi}}{n_{c+,o}\left(\sqrt{1 - \frac{\sin^2\theta_0}{n_{c+,e}^2}} - \sqrt{1 - \frac{\sin^2\theta_0}{n_{c+,o}^2}}\right)}. \tag{20}$$

From (11), (19), and (20), we find the required film thicknesses depend on the incident angle θ_0, film's refractive indices $n_{a+,e}$, $n_{a+,o}$, $n_{c+,e}$, and $n_{c+,o}$, and polarizer's average real refractive index n_p. Thus, once we know the films' and polarizer's refractive indices as well as the intended viewing angle for optimization, we can determine the required film thickness from (11), (19), and (20). By using the parameters listed in Table II and choosing $\theta_0 = 70^\circ$, the required film thicknesses, as calculated from (19) and (20), are $d_{a+} = 61.38$ μm and $d_{c+} = 101.92$ μm. Based on these film thicknesses, Fig. 14 plots the calculated iso-contrast contour of the IPS-LCD with two identical positive a-films and one positive c-film compensation. Comparing Fig. 14 with Fig. 7, we can see clearly that the viewing angle at off-axis, especially from the bisector positions $\phi_0 = 0^\circ$, 90°, 180°, and 270°, is dramatically improved. Meanwhile, the contrast ratios at on-axis, i.e., $\phi_0 = 45^\circ$, 135°, 225°, and 315° remains unchanged.

In fact, this compensation scheme can be modified by replacing those two positive a-films and one positive c-film with two negative a-films and one negative c-film, as shown in Fig. 15(a). Still, the compensation mechanism, as shown in Fig. 15(b), is similar to that with two positive a-films and one positive c-film except now the rotation on Poincaré sphere becomes counterclockwise. The required film thickness can still be determined by (19) and (20) except: (1) substituting λ with $-\lambda$ due to the negative phase retardation of negative uniaxial film; and (2) substituting those positive films' refractive indices $n_{a+,e}$, $n_{a+,o}$, $n_{c+,e}$, and $n_{c+,o}$ with the corresponding negative films' refractive indices $n_{a-,e}$, $n_{a-,o}$, $n_{c-,e}$, and $n_{c-,o}$, respectively. Its viewing angle performance, which is almost identical to Fig. 14, is not shown here to avoid redundancy.

From Fig. 14, the overall contrast ratio almost exceeds 300:1 from all viewing directions. The viewing angle performance is more symmetric than the case with one positive a-film and one positive c-film compensation, as shown in Fig. 9. This is again due to the fact that the intermediate states (points $\mathbf{E}$ and $\mathbf{F}$) both are not only located on the great circle passing through S_2 and S_3 axes and bisecting the arc $\overline{\boldsymbol{TA}}$, but also symmetrically positioned with each other about the equator plane on Poincaré sphere.

IV. Compensation Schemes for LCD With Initially Vertical Alignment

In the WVA LCDs with initially vertical alignment, such as MVA and PVA modes, a negative dielectric anisotropic nematic

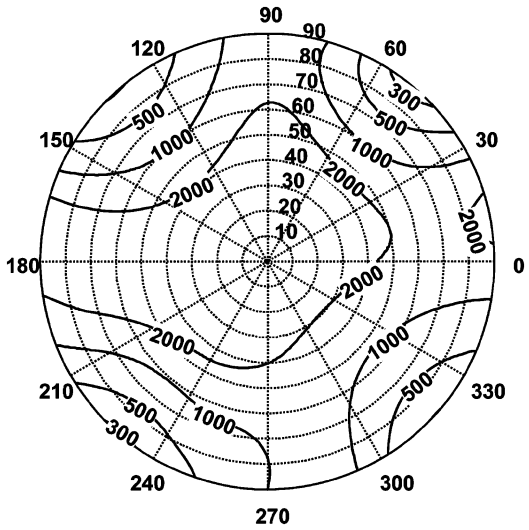

Fig. 14. Iso-contrast contour of an IPS-LCD with two identical positive a-films ($d_{a+} = 61.38\ \mu$m) and a positive c-film ($d_{c+} = 101.92\ \mu$m) under $\lambda = 550$ nm.

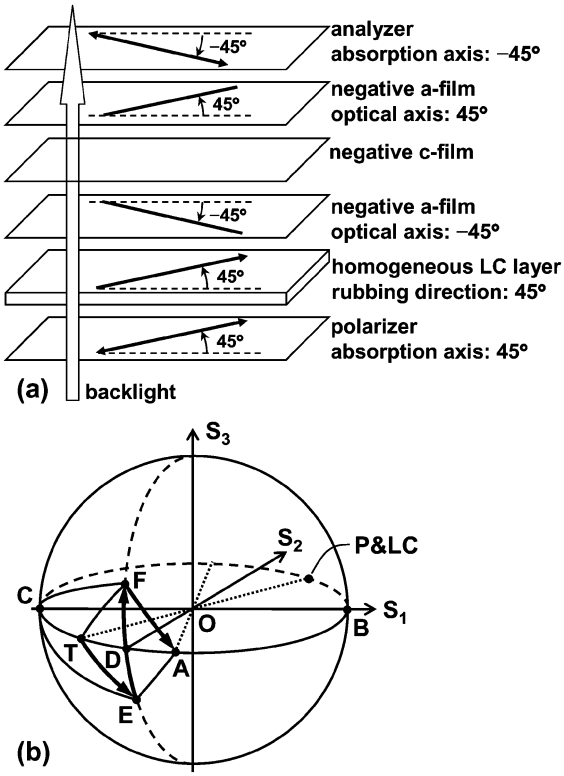

Fig. 15. (a) Device structure and (b) compensation principle of an IPS-LCD using two negative a-films and one negative c-film.

LC layer is homeotropically aligned and sandwiched between two substrates. As $V > V_{\rm th}$, the LC directors are tilted by the longitudinal electric field to be parallel to the substrate surface. Basically, both PVA and MVA modes can achieve similar director distribution; therefore, their viewing angle behaviors are quite similar. In this section, we use MVA as an example to illuminate three uniaxial-film compensation schemes and to derive their corresponding analytical solutions.

Let us assume that in each pixel the LC directors form a four-domain orientation profile, as Fig. 16(a) shows. Fig. 16(b) depicts the calculated voltage dependent transmittance curve of a typical MVA mode LCD using MLC-6608 LC material (from Merck).

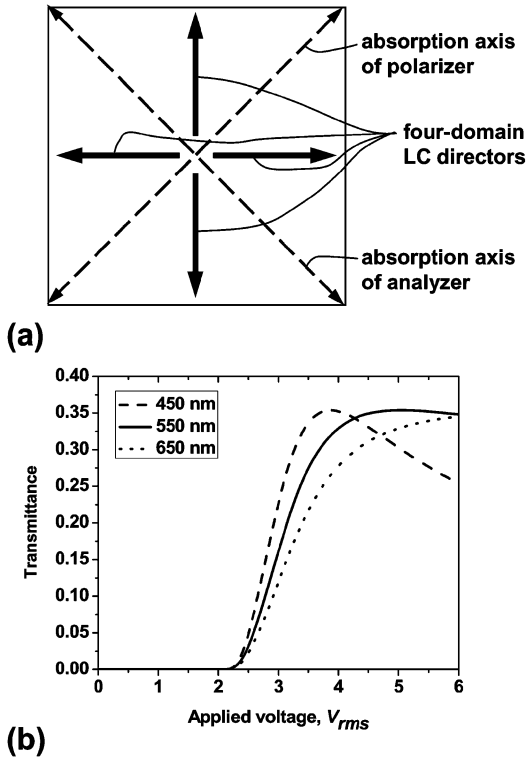

Fig. 16. (a) Schematic top-view of the four-domain LC director distribution in the voltage-on state, and (b) the voltage dependent transmittance curve of a MVA-LCD.

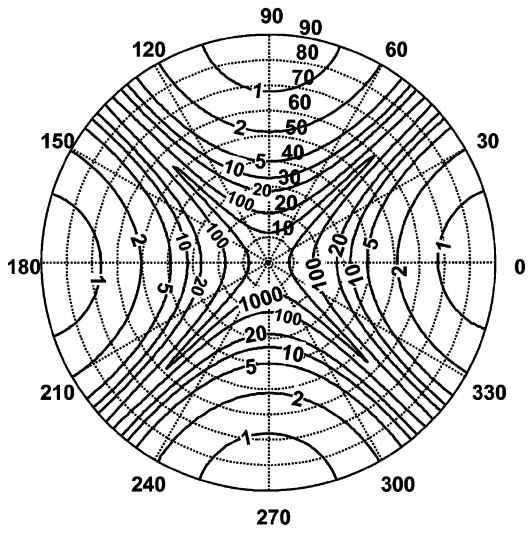

Fig. 17. Simulated iso-contrast contour of a typical four-domain MVA-LCD under $\lambda = 550$ nm.

Throughout this section, unless otherwise specified we use the parameters listed in Table III for all the calculations. The refractive indices of the uniaxial films and polarizers are still the same as listed in Table II. Fig. 17 shows the calculated iso-contrast contour of the four-domain MVA-LCD without film compensation. In the contrast ratio calculation, we first use continuum theory [20] to calculate the LC director distribution at $V_{\rm on} = 5\,{\rm V}_{\rm rms}$ and $V_{\rm off} = 0$, respectively, and then use the extended Jones matrix [15], [17] to calculate the optical transmittance for each domain and finally average all four domains up.

From Fig. 17, without compensation films the viewing angle at the bisector positions $\phi_0 = 0°$, 90°, 180°, and 270° are very poor. At these bisector viewing positions, the 10:1 contrast

TABLE III
PARAMETERS USED IN SIMULATING THE MVA-LCD VIEWING ANGLE PERFORMANCE

Parameters	Description	Values
d_{LC}	Cell gap	4.6 μm
$\theta_{pretilt}$	Surface tilt angle	89°
$n_{LC,e}$	n_e of LC material MLC−6608	1.5606
$n_{LC,o}$	n_o of LC material MLC−6608	1.4770
ϕ_1	Absorption axis of polarizer	45°
ϕ_2	Absorption axis of analyzer	−45° (or 135°)
λ	Wavelength of incident light	550 nm

ratio can only extend to $\sim 30^\circ$ polar angle. Two factors contribute to the narrow viewing angle. First, the absorption axes of the crossed polarizers are no longer perpendicular to each other at off-axis oblique viewing directions. Second, the vertically aligned LC layer behaves as a c-film, which imposes a phase retardation on the obliquely incoming linearly polarized light and modulates its polarization state. The phase retardation Γ_{LC}, which is induced by the vertically aligned LC layer at an oblique incident light, can be easily obtained from (6) as

$$\Gamma_{LC} = \frac{2\pi}{\lambda} n_{LC,o} d_{LC} \left(\sqrt{1 - \frac{\sin^2\theta_0}{n_{LC,e}^2}} - \sqrt{1 - \frac{\sin^2\theta_0}{n_{LC,o}^2}} \right). \tag{21}$$

From (21), Γ_{LC} depends on the incident angle θ_0, LC's refractive indices $n_{LC,e}$ and $n_{LC,o}$, and the LC layer's thickness d_{LC}. As an example, at incident angle $\theta_0 = 70^\circ$ the corresponding Γ_{LC}, calculated from the parameters listed in Table III, is 0.664π rad. Equation (21) will be frequently referred in this section.

In the following, we use the four-domain MVA-LCD as an example to demonstrate several uniaxial-film compensation schemes and provide each scheme a comprehensive analytical solution. All of these compensation schemes are equally applicable to PVA mode LCDs.

A. One Positive A-Film and One Negative C-Film

Fig. 18(a) shows the schematic device configuration of a MVA-LCD with one positive a-film and one negative c-film, which was first proposed by Chen [7]. As shown in the figure, the positive a-film and the negative c-film are sandwiched between the polarizer and the MVA LC layer. More specifically, the optical axis of the positive a-film is parallel to the absorption axis of the analyzer. Fig. 18(b) explains the compensation principle on Poincaré sphere when the observer views the panel from an oblique angle at the lower bisector position $\phi_0 = 270^\circ$.

The detail compensation mechanism is explained as follows, as demonstrated in Fig. 18(b). When the unpolarized light from backlight source passes the polarizer (point $\mathbf{P}$), it becomes linearly polarized and its polarization state is located at point $\mathbf{T}$, which deviates from the absorption axis of the analyzer (point $\mathbf{A}$). Then, such a linearly polarized light (point $\mathbf{T}$) successively passes through the positive a-film and the negative c-film, whose positions on the Poincaré sphere are point $\mathbf{A}$ and point $\mathbf{C}$, respectively. When the linearly polarized light (point $\mathbf{T}$) passes through the positive a-film, its polarization state is clockwise rotated from point $\mathbf{T}$ to point $\mathbf{E}$ around the $\mathbf{AO}$ axis. Point $\mathbf{E}$ is

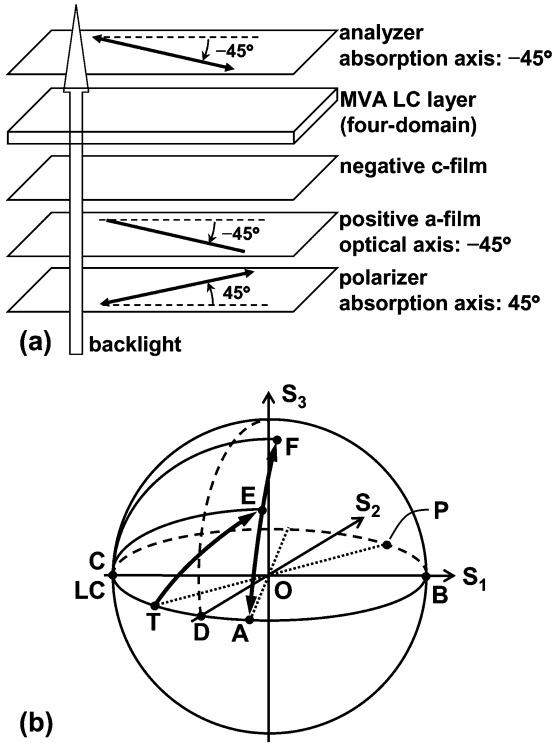

Fig. 18. (a) Device structure and (b) compensation principle of a MVA-LCD with one positive a-film and one negative c-film.

the first intermediate polarization state which, in general, is elliptical. When this elliptically polarized light traverses the negative c-film, its polarization state is counterclockwise rotated from point $\mathbf{E}$ to point $\mathbf{F}$ around the $\mathbf{CO}$ axis. Point $\mathbf{F}$ is the second intermediate polarization state, which is also elliptical. Then, this second intermediate elliptically polarized light passes through the unactivated MVA LC layer, whose position on the Poincaré sphere overlaps with point $\mathbf{C}$. Let us assume we can find the proper phase retardations of the positive a-film and negative c-film such that when the second intermediate elliptically polarized light passes through the unactivated MVA LC layer its polarization state would be rotated clockwise from point $\mathbf{F}$ to point $\mathbf{A}$ around the $\mathbf{CO}$ axis. Consequently, at $V = 0$ the light is completely absorbed by the analyzer (point $\mathbf{A}$) and a good dark state is achieved even viewed from the oblique angle at the bisector positions.

To reach the abovementioned goal, we can readily determine from Fig. 18(b) that the following three requirements must be satisfied: 1) the arc $\overline{\boldsymbol{EA}}$ should be equal to the arc $\overline{\boldsymbol{TA}}$; 2) the arcs $\overline{\boldsymbol{AC}}$, $\overline{\boldsymbol{EC}}$, and $\overline{\boldsymbol{FC}}$ all should be equal to each other; and 3) the spherical angle $\angle\boldsymbol{ACF}$ is the sum of the spherical angles $\angle\boldsymbol{ACE}$ and $\angle\boldsymbol{ECF}$. Besides, from Fig. 18(b), we also find that $\angle\boldsymbol{POB} = \angle\boldsymbol{AOB} = \varphi, \overline{\boldsymbol{TA}} = \pi - 2\varphi$, and $\overline{\boldsymbol{AC}} = \pi - \varphi$. Based on the spherical trigonometry, we can derive the following relationships from the spherical triangles $\boldsymbol{CAE}$ and $\boldsymbol{CAF}$

$$\angle EAC = \cos^{-1}(-\mathrm{ctg}^2\varphi) \tag{22a}$$

$$\angle ACE = 2\sin^{-1}(\mathrm{ctg}\varphi) \tag{22b}$$

where φ, determined by (11), is the effective polarizer angle on the wave plane from the lower bisector viewing position $\phi_0 = 270^\circ$.

Since the required positive a-film's phase retardation Γ_{a+} equals to the spherical angle $\angle \boldsymbol{EAT} (= \angle \boldsymbol{EAC})$, thus from (5) and (22a) the positive a-film's thickness d_{a+} is found to be:

$$d_{a+} = \lambda \frac{\frac{\cos^{-1}(-\mathrm{ctg}^2\varphi)}{2\pi}}{n_{a+,e}\sqrt{1-\frac{\sin^2\theta_0}{2n_{a+,e}^2}-\frac{\sin^2\theta_0}{2n_{a+,o}^2}}-n_{a+,o}\sqrt{1-\frac{\sin^2\theta_0}{n_{a+,o}^2}}}. \tag{23}$$

In the derivation of (23), we substitute $\phi_n = -45^\circ$ and $\phi_0 = 270^\circ$ into (5) because the positive a-film's optical axis is oriented at -45° direction, as Fig. 18(a) shows, and the viewing direction is from $\phi_0 = 270^\circ$ azimuthal angle.

On the other hand, the required negative c-film's phase retardation Γ_{c-} equals to the negative spherical angle $\angle \boldsymbol{ECF}$, *i.e.*, $\Gamma_{c-} = -\angle \boldsymbol{ECF} = \angle \boldsymbol{ACE} - \angle \boldsymbol{ACF}$. The spherical angle $\angle \boldsymbol{ACF}$ is equal to the unactivated MVA-LC layer's phase retardation Γ_{LC} as in (21). This is because the function of the unactivated MVA LC layer is to clockwise rotate around the $\mathbf{CO}$ axis from point $\mathbf{F}$ to point $\mathbf{A}$. Thus from (6) and (22b) we can obtain the required negative c-film's thickness d_{c-} as

$$d_{c-} = \lambda \frac{\frac{2\sin^{-1}(\mathrm{ctg}\varphi)-\Gamma_{LC}}{2\pi}}{n_{c-,o}\left(\sqrt{1-\frac{\sin^2\theta_0}{n_{c-,e}^2}}-\sqrt{1-\frac{\sin^2\theta_0}{n_{c-,o}^2}}\right)} \tag{24}$$

where Γ_{LC} is given by (21).

As we can see from (11), (21), (23), and (24), for a given MVA LC cell, the required film thicknesses depend on the incident angle θ_0, film's refractive indices $n_{c-,e}$, $n_{c-,o}$, $n_{a+,e}$, and $n_{a+,o}$, and polarizer's average real refractive index n_p. Therefore, once we know both the films' and polarizer's refractive indices as well as the intended viewing angle or incident angle, we can determine the compensation films' thickness from (11), (21), (23), and (24). For example, if we want to optimize the LCD viewing angle at $\theta_0 = 70^\circ$, then we can plug in the parameters listed in Tables II and III into (23) and (24) and find $d_{a+} = 92.59$ μm and $d_{c-} = 186.08$ μm. Based on the obtained film thicknesses, Fig. 19 depicts the calculated iso-contrast contour of an MVA-LCD compensated by one positive a-film and one negative c-film. Comparing Fig. 19 with Fig. 17, we can clearly see that the viewing angle performance at off-axis viewing directions, especially the bisector positions $\phi_0 = 0^\circ$, 90°, 180°, and 270°, is dramatically improved. In the mean time, the contrast ratios at on-axis viewing directions ($\phi_0 = 45^\circ$, 135°, 225°, and 315°) remain the same.

This compensation scheme can be modified by exchanging the positions of the negative c-film and the MVA LC layer. In other words, the incident light passes through the MVA LC layer first before it enters the negative c-film. In this case, the required film thickness can still be determined by (23) and (24), and the resultant viewing angle performance is nearly identical to Fig. 19.

In addition, this compensation scheme can be further modified by placing the positive a-film and negative c-film between the MVA LC layer and the analyzer, as Fig. 20(a) shows. Different from Fig. 18(a), now the positive a-film is adjacent to the analyzer and its optical axis is perpendicular to the absorption axis of the analyzer. Fig. 20(b) shows the compensation principle of the modified device. Following the same procedures,

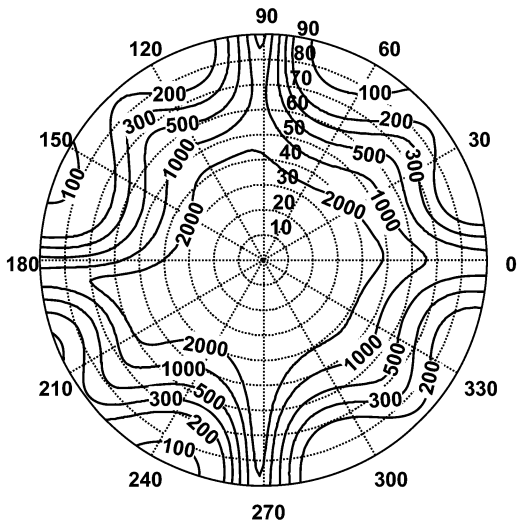

Fig. 19. Simulated iso-contrast contour of an MVA-LCD with a positive a-film ($d_{a+} = 92.59$ μm) and a negative c-film ($d_{c-} = 186.08$ μm) under $\lambda = 550$ nm.

we can readily determine from Fig. 20(b) that the required film thicknesses are identical to (23) and (24). The resultant viewing angle is almost the same as Fig. 19.

As shown in Fig. 19, with film compensation the 100:1 contrast ratio barely exceeds $\sim 75^\circ$ polar angle. This viewing angle performance is not as good as compared to the results obtained for IPS-LCDs as described in Section III. This is due to the fact that the intermediate states, points $\mathbf{E}$ and $\mathbf{F}$, are not located on the great circle which passes through S_2 and S_3 axes. In Sections IV-B and C, we will describe two compensation schemes in which the intermediate states are located on the great circle passing through S_2 and S_3 axes and bisecting the arc $\overline{\boldsymbol{TA}}$.

B. One Positive A-Film, One Negative A-Film, and One Negative C-Film

Fig. 21(a) shows the schematic device configuration of a MVA-LCD with one positive a-film, one negative a-film, and one negative c-film. As shown in the figure, the positive a-film is located between the polarizer and the MVA LC layer, while the negative a-film and negative c-film are sandwiched between the MVA LC layer and the analyzer. More specifically, the optical axis of the positive a-film is parallel to the absorption axis of the analyzer, and the optical axis of the negative a-film is parallel to the absorption axes of the polarizer. Fig. 21(b) explains the compensation principle on Poincaré sphere when the observer views the LCD panel from an oblique angle at the lower bisector position $\phi_0 = 270^\circ$.

The detailed compensation mechanism is explained based on Fig. 21(b). When the unpolarized light from backlight passes through the polarizer (point $\mathbf{P}$), it becomes linearly polarized and its polarization state is located at point $\mathbf{T}$, which deviates from the absorption axis of the analyzer (point $\mathbf{A}$). Afterwards, the linearly polarized light (point $\mathbf{T}$) traverses the positive a-film, whose position on the Poincaré sphere overlaps with point $\mathbf{A}$, and its polarization state is rotated clockwise from point $\mathbf{T}$ to point $\mathbf{E}$ around the $\mathbf{AO}$ axis. Point $\mathbf{E}$ is the first intermediate elliptical polarization state.

To obtain a symmetric viewing angle, we intentionally let the point $\mathbf{E}$ locate on the great circle passing through S_2 and S_3 axes

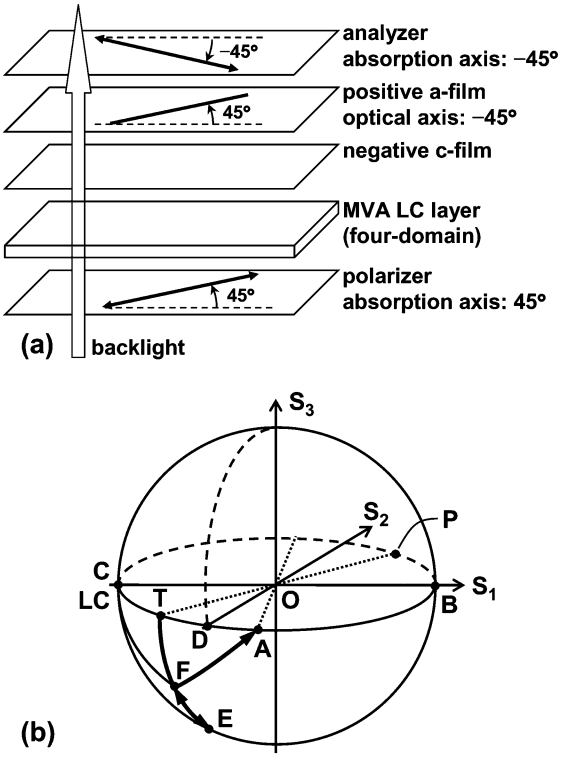

Fig. 20. (a) An alternative device structure and (b) compensation principle of the MVA-LCD using a negative c-film and a positive a-film.

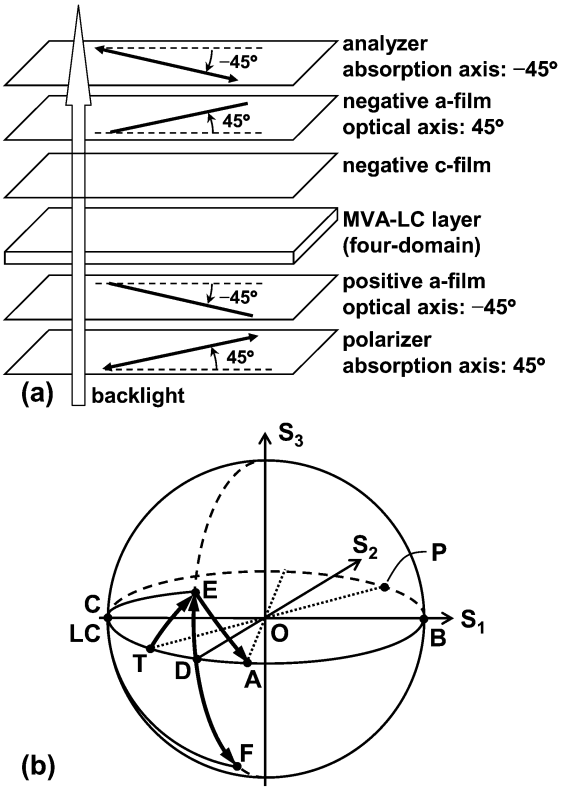

Fig. 21. (a) Device structure and (b) compensation principle of an MVA-LCD with one positive a-film, one negative a-film, and one negative c-film.

and bisecting the arc $\overline{TA}$. Then this elliptically polarized light successively enters the unactivated MVA LC layer and the negative c-film, whose positions on the Poincaré sphere are both at point $\mathbf{C}$. When the elliptically polarized light passes through the unactivated MVA LC layer, its polarization state is clockwise rotated around the $\mathbf{CO}$ axis from point $\mathbf{E}$ to point $\mathbf{F}$. Point $\mathbf{F}$ is the second intermediate elliptical polarization state, which is also located on the same great circle passing through S_2 and S_3 axes. Then this second intermediate elliptically polarized light hits the negative c-film. If the phase retardation of the negative c-film is such designed that when the second intermediate elliptically polarized light passes through the negative c-film its polarization state will be rotated counterclockwise around the $\mathbf{CO}$ axis from point $\mathbf{F}$ back to point $\mathbf{E}$. Now point $\mathbf{E}$ represents the third intermediate elliptical polarization state. After that, this third elliptically polarized light passes through the negative a-film, whose position on the Poincaré sphere overlaps with point $\mathbf{P}$. If the phase retardation of the negative a-film is properly chosen such that when the third intermediate elliptically polarized light (point $\mathbf{E}$) passes through the negative a-film its polarization state can be rotated counterclockwise around the $\mathbf{PO}$ axis from point $\mathbf{E}$ to point $\mathbf{A}$. Consequently, the light is completely absorbed by the analyzer (point $\mathbf{A}$) and a good dark state is achieved even if it is viewed from the bisector directions.

To determine each film's thickness, from Fig. 21(b) we find that the following two requirements must be satisfied: 1) the arcs of $\overline{\boldsymbol{EA}}$, $\overline{\boldsymbol{ET}}$, and $\overline{\boldsymbol{TA}}$ should be all equal and 2) the arc $\overline{\boldsymbol{EF}}$ is located on the great circle passing through S_2 and S_3 axes and bisecting the arc $\overline{\boldsymbol{TA}}$. That implies the spherical triangle $\boldsymbol{ETA}$ is an equilateral spherical triangle. Besides, from Fig. 21(b), we also obtain $\angle\boldsymbol{POB} = \angle\boldsymbol{AOB} = \varphi$ and $\overline{\boldsymbol{TA}} = \pi - 2\varphi$. Based on the spherical trigonometry, we derive the following relationships from the equilateral spherical triangle $\boldsymbol{ETA}$:

$$\angle EAT = \angle ETA = \cos^{-1}(-\mathrm{ctg}\varphi \cdot \mathrm{ctg}2\varphi) \tag{25}$$

where φ, determined by (11), is the effective polarizer angle on the wave plane as viewing from the lower bisector direction ($\phi_0 = 270°$).

Since the required positive a-film's phase retardation Γ_{a+} equals to the spherical angle $\angle\boldsymbol{EAT}$, thus from (5) and (25) the required positive a-film's thickness d_{a+} can be expressed as:

$$d_{a+} = \lambda \frac{\frac{\cos^{-1}(-\mathrm{ctg}\varphi\cdot\mathrm{ctg}2\varphi)}{2\pi}}{n_{a+,e}\sqrt{1-\frac{\sin^2\theta_0}{2n_{a+,e}^2}-\frac{\sin^2\theta_0}{2n_{a+,o}^2}} - n_{a+,o}\sqrt{1-\frac{\sin^2\theta_0}{n_{a+,o}^2}}}. \tag{26}$$

In the process of deriving (26), we substitute $\phi_n = -45°$ and $\phi_0 = 270°$ into (5) because the positive a-film's optical axis is oriented at $-45°$ direction, as Fig. 21(a) shows, and the viewing direction is from $\phi_0 = 270°$ azimuthal angle.

Similarly, the required negative a-film's phase retardation Γ_{a-} is equal to the negative spherical angle $\angle\boldsymbol{ETA}$, *i.e.*, $\Gamma_{a-} = -\angle\boldsymbol{ETA}$. Thus, from (5) and (25) we derive the negative a-film's thickness d_{a-} as

$$d_{a-} = -\lambda \frac{\frac{\cos^{-1}(-\mathrm{ctg}\varphi\cdot\mathrm{ctg}2\varphi)}{2\pi}}{n_{a-,e}\sqrt{1-\frac{\sin^2\theta_0}{2n_{a-,e}^2}-\frac{\sin^2\theta_0}{2n_{a-,o}^2}} - n_{a-,o}\sqrt{1-\frac{\sin^2\theta_0}{n_{a-,o}^2}}}. \tag{27}$$

Here we substitute $\phi_n = 45°$ and $\phi_0 = 270°$ into (5) because the negative a-film's optical axis is oriented at 45° direction, as

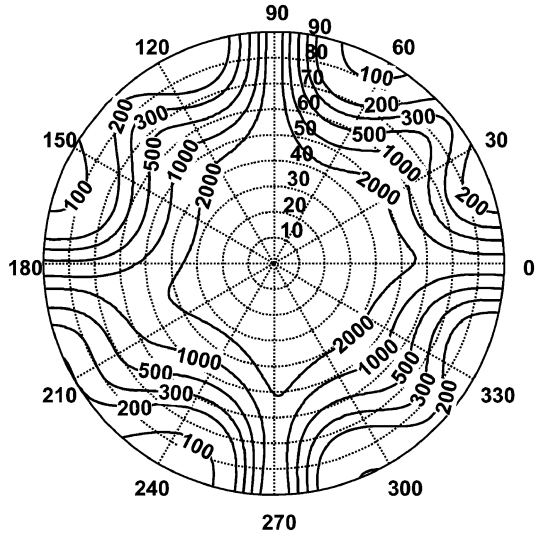

Fig. 22. Iso-contrast contour of an MVA-LCD with one positive a-film ($d_{a+} = 61.38\,\mu$m), one negative a-film ($d_{a-} = 61.37\,\mu$m), and one negative c-film ($d_{c-} = 246.11\,\mu$m) under $\lambda = 550$ nm.

Fig. 21(a) shows, and the viewing direction is from $\phi_0 = 270°$ azimuthal angle.

To obtain the negative c-film's thickness, we need to find its phase retardation Γ_{c-} first. From the compensation mechanism, it is easy to find that $\Gamma_{c-} = -\Gamma_{LC}$ since the unactivated MVA LC layer's role it is to rotate clockwise around the $\mathbf{CO}$ axis from point $\mathbf{E}$ to point $\mathbf{F}$. On the other hand, the negative c-film's function is to counterclockwise rotate around the $\mathbf{CO}$ axis from point $\mathbf{F}$ back to point $\mathbf{E}$. Therefore, from (6) we derive the required negative c-film's thickness d_{c-} as

$$d_{c-} = -\lambda \frac{\frac{\Gamma_{LC}}{2\pi}}{n_{c-,o}\left(\sqrt{1-\frac{\sin^2\theta_0}{n^2_{c-,e}}} - \sqrt{1-\frac{\sin^2\theta_0}{n^2_{c-,o}}}\right)} \tag{28}$$

where Γ_{LC} is determined by (21).

From (11), (21), and (26)–(28), we find that for a given MVA LC cell the required film thicknesses depend on the incident angle θ_0, film's refractive indices $n_{a+,e}$, $n_{a+,o}$, $n_{a-,e}$, $n_{a-,o}$, $n_{c-,e}$, and $n_{c-,o}$, and polarizer's average real refractive index n_p.Therefore, once we know the films' and polarizer's refractive indices and the intended viewing angle (θ_0) for optimizing the LCD panel, we can determine the compensation films' thickness from (11), (21), and (26)–(28). For instance, if we choose $\theta_0 = 70°$ and use the parameters listed in Tables II and III, then we can calculate the required film thicknesses from (26)–(28). Results are $d_{a+} = 61.38\ \mu$m, $d_{a-} = 61.37\mu$m, and $d_{c-} = 246.11\ \mu$m. Based on these film thicknesses, Fig. 22 plots the simulated iso-contrast contour for an MVA-LCD with one positive a-film, one negative a-film, and one negative c-film. Comparing Fig. 22 with Fig. 17, we can clearly see that the viewing angle at off-axis viewing directions, especially the bisector positions ($\phi_0 = 0°$, {\rm 90}°, {\rm 180}°, and {\rm 270}°), is dramatically improved. At the same time, the contrast ratios at on-axis, i.e., $\phi_0 = 45°$, {\rm 135}°, {\rm 225}°, and {\rm 315}°, remain unchanged.

This compensation scheme can be modified by exchanging the positions of the negative c-film and the MVA LC layer while keeping both positive and negative a-films unchanged. In other words, the incident light passes through the negative c-film first before it enters the MVA LC layer. Under such a circumstance, the required film thickness can still be found from (26)–(28), and the resultant iso-contrast contour is nearly identical to Fig. 22.

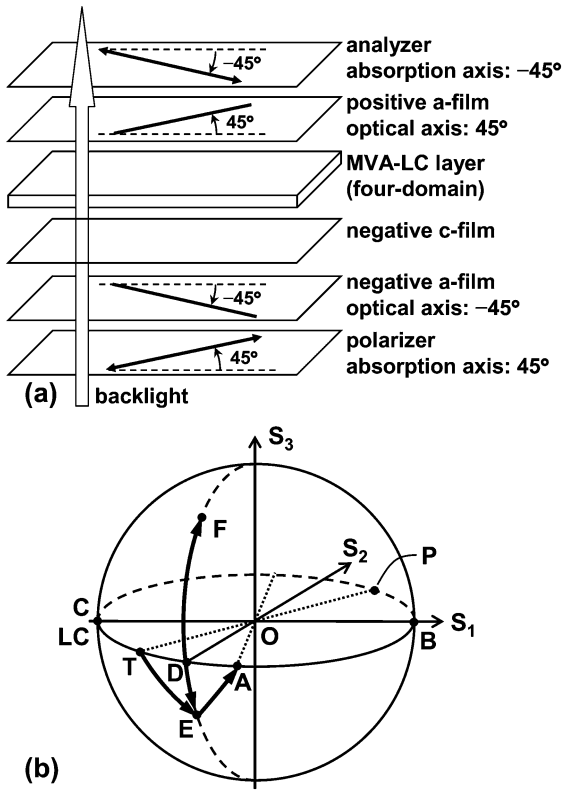

Fig. 23. (a) An alternative device structure and (b) compensation principle of an MVA-LCD with one positive a-film, one negative a-film, and one negative c-film.

Another alternative is to exchange the positions of both positive a-film and negative a-film, as shown in Fig. 23(a).Different from the device configuration sketched in Fig. 21(a), now the positive a-film is adjacent to the analyzer while the negative a-film is adjacent to the polarizer. The corresponding compensation mechanism is illustrated in Fig. 23(b). Following the same analysis as above, we can readily determine from Fig. 23(b) that the required film thicknesses are identical to (26)–(28). The resultant iso-contrast contour is almost the same as Fig. 22 and is, thus, not shown here to avoid redundancy.

From Fig. 22, the 100:1 iso-contrast contours barely exceed $\sim 75°$ polar angle. Although the two intermediate polarization states, points $\mathbf{E}$ and $\mathbf{F}$, are located on the great circle which passes through S_2 and S_3 axes, these two intermediate states are not symmetrically located with respect to the equator plane. In Section IV-C, we will describe a compensation scheme in which the intermediate states are not only located on the great circle passing through S_2 and S_3 axes and bisecting the arc $\overline{TA}$, but also symmetrically located to with respect to the equator plane.

C. Two Positive A-Films and Two Negative C-Films

Fig. 24(a) shows the schematic device configuration of an MVA-LCD with two positive a-films and two negative c-films, which was first proposed by Hong *et al.* [9]. As shown in the

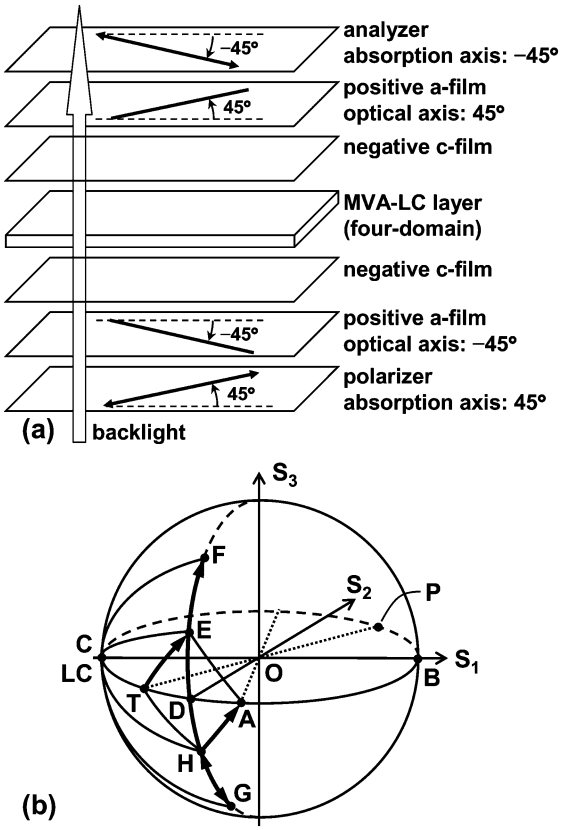

Fig. 24. (a) Device structure and (b) compensation principle of an MVA-LCD with two positive a-films and two negative c-films.

figure, on each side of the MVA LC layer, there is one pair of positive a-film and negative c-film. Both negative c-films are adjacent to the MVA LC layer. More specifically, the optical axis of the bottom positive a-film is parallel to the absorption axis of the analyzer, while the optical axis of the top positive a-film is parallel to the absorption axis of the polarizer. Fig. 24(b) explains the compensation principle on Poincaré sphere when the observer views the panel from an oblique angle at the lower bisector position, i.e., $\phi_0 = 270°$.

The detailed compensation mechanism is explained as follows based on Fig. 24(b). When the unpolarized light from backlight passes the polarizer (point $\mathbf{P}$), it becomes linearly polarized, and its polarization state is located at point $\mathbf{T}$ which deviates from the absorption axis of the analyzer (point $\mathbf{A}$). Successively, such a linearly polarized light (point $\mathbf{T}$) goes through the bottom positive a-film and the bottom negative c-film, whose positions on the Poincaré sphere are point $\mathbf{A}$ and point $\mathbf{C}$, respectively. When the linearly polarized light (point $\mathbf{T}$) traverses the bottom positive a-film, its polarization state is rotated clockwise around the $\mathbf{AO}$ axis and changed from point $\mathbf{T}$ to point $\mathbf{E}$. Point $\mathbf{E}$ is the first intermediate polarization state. More specifically, it is an elliptical polarization state. To obtain a symmetric viewing angle, we intentionally let the point $\mathbf{E}$ be located on the great circle passing through S_2 and S_3 axes and bisecting the arc $\overline{\boldsymbol{TA}}$. When this elliptically polarized light penetrates the bottom negative c-film, its polarization state is counterclockwise rotated around the $\mathbf{CO}$ axis changing point $\mathbf{E}$ to point $\mathbf{F}$. Point $\mathbf{F}$ is the second intermediate elliptical polarization state, which is also located on the same great circle as point $\mathbf{E}$ does. Afterwards, this second intermediate elliptically polarized light passes through the unactivated MVA LC layer, whose position on the Poincaré sphere overlaps with point $\mathbf{C}$. Thus its polarization state is clockwise rotated around the $\mathbf{CO}$ axis moving point $\mathbf{F}$ to point $\mathbf{G}$. Point $\mathbf{G}$ is the third intermediate elliptical polarization state, which again is located on the same great circle as points $\mathbf{E}$ and $\mathbf{F}$ do. Now this third intermediate elliptically polarized light (point $\mathbf{G}$) successively passes through the top negative c-film and the top positive a-film, whose positions on the Poincaré sphere are point $\mathbf{C}$ and point $\mathbf{P}$, respectively. When the third intermediate polarized light passes through the top negative c-film, its polarization state is rotated counterclockwise around the $\mathbf{CO}$ axis changing point $\mathbf{G}$ to point $\mathbf{H}$. Point $\mathbf{H}$ is the fourth intermediate elliptical polarization state, which is once again located on the same great circle as points $\mathbf{E}$, $\mathbf{F}$, and $\mathbf{G}$ do. When the fourth intermediate elliptically polarized light passes through the top positive a-film, its polarization state can be rotated clockwise around the $\mathbf{PO}$ axis moving point $\mathbf{H}$ to point $\mathbf{A}$, provided that we properly design the phase retardation values of all four uniaxial films. As a result, at the voltage-off state the light is completely absorbed by the analyzer (point $\mathbf{A}$) resulting in a good dark state even if it is viewed from the bisector directions.

As mentioned above, to keep symmetric viewing angle all the four intermediate polarization states must be located on the great circle passing through S_2 and S_3 axes and bisecting the arc $\overline{\boldsymbol{TA}}$. Moreover, the first (point $\mathbf{E}$) and the fourth (point $\mathbf{H}$) intermediate polarization states should be symmetric to each other with respect to the equator plane, and the second (point $\mathbf{F}$) and the third (point $\mathbf{G}$) intermediate polarization states should also be symmetric to each other with respect to the equator plane. From the Poincaré sphere, we find that the arcs $\overline{\boldsymbol{ET}}$, $\overline{\boldsymbol{EA}}$, $\overline{\boldsymbol{TA}}$, $\overline{\boldsymbol{HT}}$, and $\overline{\boldsymbol{HA}}$ should all be equal to each other. In other words, both spherical triangles $\boldsymbol{ETA}$ and $\boldsymbol{HTA}$ are equilateral spherical triangles. In addition, we can also obtain $\overline{\boldsymbol{CF}} = \overline{\boldsymbol{CE}} = \overline{\boldsymbol{CD}} = \overline{\boldsymbol{CH}} = \overline{\boldsymbol{CG}} = \pi/2$, $\angle \boldsymbol{POB} = \angle \boldsymbol{AOB} = \varphi$, and $\overline{\boldsymbol{TA}} = \pi - 2\varphi$ from Fig. 23(b).

Based on spherical trigonometry, we can derive the following relationships from the isosceles spherical triangle $\boldsymbol{CDE}$ and $\boldsymbol{CDH}$, as well as the equilateral spherical triangles $\boldsymbol{ETA}$ and $\boldsymbol{HTA}$:

$$\angle EAT = \angle ATH = \cos^{-1}(-\mathrm{ctg}\varphi \cdot \mathrm{ctg}2\varphi) \tag{29a}$$

$$\angle ECD = \angle HCD = \cos^{-1}\left(\frac{-\cos 2\varphi}{\sin\varphi}\right) \tag{29b}$$

where φ, determined by (11), is the effective polarizer angle on the wave plane from the lower bisector viewing position, i.e., $\varphi_0 = 270°$. Moreover, from the abovementioned compensation principle and the symmetry feature of points $\mathbf{F}$ and $\mathbf{G}$ with respect to the equator plane, we have

$$\angle FCD = \angle GCD = \frac{\Gamma_{LC}}{2}, \tag{29c}$$

where Γ_{LC} is the phase retardation introduced by the unactivated MVA LC layer at an oblique incident light, as expressed in (21).

To calculate the thickness of each compensation film, the following information is useful. The bottom positive a-film's phase retardation is equal to the spherical angle $\angle \boldsymbol{EAT}$, while the top positive a-film's phase retardation is equal to the spherical angle $\angle \boldsymbol{ATH}$. Thus, the required film thicknesses for both positive a-films should be equal to each other, as indicated by (29a). From (5) and (29a), the required film thickness d_{a+} for both positive a-films is expressed as

$$d_{a+} = \lambda \frac{\frac{\cos^{-1}(-\mathrm{ctg}\varphi \cdot \mathrm{ctg}2\varphi)}{2\pi}}{n_{a+,e}\sqrt{1-\frac{\sin^2\theta_0}{2n_{a+,e}^2}-\frac{\sin^2\theta_0}{2n_{a+,o}^2}}-n_{a+,o}\sqrt{1-\frac{\sin^2\theta_0}{n_{a+,o}^2}}}. \tag{30}$$

In the derivation of (30), we substitute $\phi_n = \pm 45^\circ$ and $\phi_0 = 270^\circ$ into (5) because the positive a-films' optical axes are oriented at either 45° or −45° directions, as Fig. 24(a) shows, and the viewing direction is from $\varphi_0 = 270^\circ$ azimuthal angle.

To obtain the required negative c-film's thickness, we need to determine its phase retardation first. From Fig. 24(b), the required bottom negative c-film's phase retardation equals to the negative spherical angle $\angle \boldsymbol{ECF}$, while the required top negative c-film's phase retardation equals to the negative spherical angle $\angle \boldsymbol{HCG}$. As a result, the required film thickness for both negative c-films should equal to each other, as indicated by (29b) and (29c). Accordingly, the required phase retardation for both negative c-films is $\Gamma_{c-} = -\angle \boldsymbol{ECF} = -\angle \boldsymbol{HCG} = \angle \boldsymbol{ECD} - \angle \boldsymbol{FCD} = \angle \boldsymbol{HCD} - \angle \boldsymbol{GCD}$. Thus from (6), (29b), and (29c), the required film thickness d_{c-} for both negative c-films has the following expression:

$$d_{c-} = \lambda \frac{\frac{\cos^{-1}\left(\frac{-\cos 2\varphi}{\sin\varphi}\right)-\frac{\Gamma_{LC}}{2}}{2\pi}}{n_{c-,o}\left(\sqrt{1-\frac{\sin^2\theta_0}{n_{c-,e}^2}}-\sqrt{1-\frac{\sin^2\theta_0}{n_{c-,o}^2}}\right)} \tag{31}$$

where Γ_{LC} is given by (21).

As seen from (11), (21), (30), and (31), for a given MVA LC cell, the required film thicknesses depend on the incident angle (θ_0), film's refractive indices $n_{a+,e}$, $n_{a+,o}$, $n_{c-,e}$, and $n_{c-,o}$, and polarizer's average real refractive index n_p. Therefore, once we know both films' and polarizer's refractive indices as well as the intended viewing angle for optimizing the LCD panel, we can determine the required compensation films' thickness from (11), (21), (30), and (31). For instance, if we set $\theta_0 = 70^\circ$ and use the parameters listed in Tables II and III, we could calculate the required film thicknesses from (30) and (31). Results are found to be $d_{a+} = 61.38\ \mu$m and $d_{c-} = 72.14\ \mu$m. Using these film thicknesses, we can calculate the iso-contrast contour for the MVA-LCD using two positive a-films and two negative c-films. Results are plotted in Fig. 25. Comparing Fig. 25 with Fig. 17, we can clearly see that the viewing angle performance at off-axis viewing directions, especially the bisector positions ($\phi_0 = 0^\circ$, 90°, 180°, and 270°), is dramatically improved. In the mean time, the contrast ratios at on-axis viewing directions ($\phi_0 = 45^\circ$, 135°, 225°, and 315°) remain the same.

This compensation scheme can be modified by replacing both positive a-films with negative a-films while keeping their optical axis directions unchanged. The schematic device configuration is shown in Fig. 26(a) and the corresponding compensation principle is illustrated in Fig. 26(b). Now the bottom negative a-film's function is to counterclockwise rotate around the $\mathbf{AO}$ axis and move point $\mathbf{T}$ to point $\mathbf{E}$, while the bottom negative c-film's function is to counterclockwise rotate around the $\mathbf{CO}$ axis and moving point $\mathbf{E}$ to point $\mathbf{F}$. Next, the unactivated MVA LC layer clockwise rotates around the $\mathbf{CO}$ axis moving point $\mathbf{F}$ to point $\mathbf{G}$, and the top negative c-film counterclockwise rotates around the $\mathbf{CO}$ axis which moves point $\mathbf{G}$ to point $\mathbf{H}$. Finally, the top negative a-film counterclockwise rotates around the $\mathbf{PO}$ axis moving point $\mathbf{H}$ to point $\mathbf{A}$, which is the absorption direction of the analyzer.

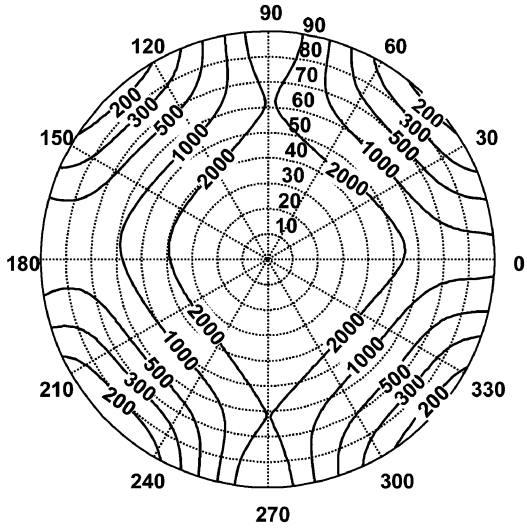

Fig. 25. Contrast ratio contour plot of an MVA-LCD with two identical positive a-films ($d_{a+} = 61.38\ \mu$m) and two identical negative c-film ($d_{c-} = 72.14\ \mu$m) under $\lambda = 550$ nm.

Following the same analysis, we can obtain the required negative a-film's thickness d_{a-} as

$$d_{a-} = -\lambda \frac{\frac{\cos^{-1}(-\mathrm{ctg}\varphi \cdot \mathrm{ctg}2\varphi)}{2\pi}}{n_{a-,e}\left(\sqrt{1-\frac{\sin^2\theta_0}{2n_{a-,e}^2}-\frac{\sin^2\theta_0}{2n_{a-,o}^2}}\right)-n_{a-,o}\sqrt{1-\frac{\sin^2\theta_0}{n_{a-,o}^2}}} \tag{32}$$

and the required negative c-film's thickness d_{c-} as

$$d_{c-} = -\lambda \frac{\frac{\cos^{-1}(\frac{-\cos 2\varphi}{\sin\varphi})+\frac{\Gamma_{LC}}{2}}{2\pi}}{n_{c-,o}\sqrt{1-\frac{\sin^2\theta_0}{n_{c-,e}^2}}-\sqrt{1-\frac{\sin^2\theta_0}{n_{c-,o}^2}}}. \tag{33}$$

By using the parameters listed in Tables II and III and set $\theta_0 = 70^\circ$ as the intended viewing cone for optimization, the required film thicknesses as calculated from (32) and (33) are $d_{a-} = 61.37\ \mu$m and $d_{c-} = 173.96\ \mu$m, respectively. The resultant iso-contrast contour is quite similar to Fig. 25 and is not shown here to avoid redundancy.

As shown in Fig. 25, in this compensation scheme, the off-axis viewing angle is better than the on-axis one. This is due to the facts that (1) all four intermediate polarization states are located on the same great circle passing through S_2 and S_3 axes and bisecting the arc $\overline{\boldsymbol{TA}}$, and (2) the first and the fourth intermediate states are symmetrical to each other with respect to the equator plane, and so are the second and the third intermediate states.

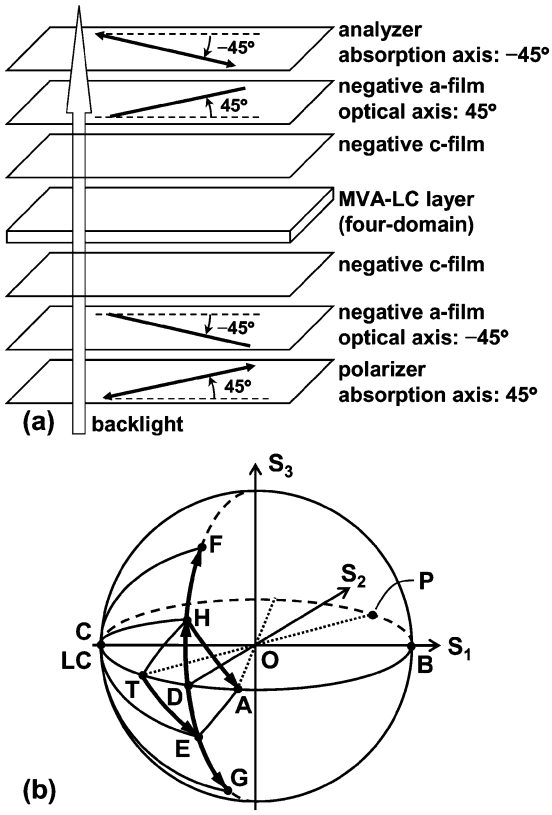

Fig. 26. (a) Device configuration and (b) compensation principle of an MVA-LCD incorporating two negative a-films and two negative c-films for phase compensation.

V. Discussion

A. General Compensation Rules

Although we have described several compensation schemes for both IPS- and MVA- LCDs, it is still possible to modify the polarization state change routes on the Poincaré sphere and develop different compensation methods. However, some general guidelines should be observed in order to obtain good viewing characteristics.

First, it is advisable to keep all the intermediate polarization states located on the great circle passing through S_2 and S_3 axes to ensure a more symmetric viewing characteristic. Second, to avoid degrading the on-axis viewing angle, the optical axis of the a-films should be either parallel or perpendicular to the absorption axes of the polarizer and the analyzer. Third, if the uniaxial a-film, either positive or negative, is placed adjacent to the polarizer or the analyzer, the uniaxial a-film's optical axis should be perpendicular to the absorption axis of the adjacent polarizer or analyzer. Otherwise, the uniaxial film cannot perform its compensation role. Fourth, in the IPS and FFS modes, the homogenously aligned LC layer is preferred to be adjacent to the entrance polarizer and its rubbing direction should be parallel to the absorption axis of the entrance polarizer. Under such a circumstance, the homogeneously aligned LC layer does not modulate the polarization state of the obliquely incident light (even from off-axis viewing directions). Consequently, the required compensation film's thickness is insensitive to the LC cell gap variation.

B. Wavelength Dependence

The derived film thickness is dependent on the incident light wavelength. Throughout our discussions, we only use 550 nm monochromatic light as an example to demonstrate the design principles. In a full-color display, red, green, and blue colors are present. The required film thickness is slightly different for each color. However, since human eye's photopic response is most sensitive to green light, the example of using 550 nm monochromatic light is still of practical significance. Of course, under white light illumination the resultant viewing angle will be slightly worse than those results calculated using $\lambda = 550$ nm.

C. Other Effects

In the actual LCD device, both sides of the sheet polarizer are protected by triacetate cellulose (TAC) films. Such a TAC film renders a negative c-film effect. Therefore, in the actual LCD device, there is a built-in effective negative c-film ($d\Delta n \sim 40$ nm) on the inner side of the polarizer and the analyzer. These two built-in negative c-films may change the polarization state of the obliquely incident light. Consequently, the required film thickness might not be exactly the same as we obtained from the analytical solutions. However, one can always follow the same analysis procedures to find solutions. The analytical solutions, although have increased complexity, are still obtainable based on the spherical trigonometry.

VI. Conclusion

The uniaxial-film-compensated WVA LCDs with initially homogeneous and vertical alignments are analyzed with the illustration of Poincaré sphere representation. For each compensation scheme, a detailed compensation principle is explained based on the polarization state change on the Poincaré sphere. From spherical trigonometry, we derive the analytical solutions for each scheme. These analytical solutions not only shed light for understanding the underlying phase compensation principles but also represent straightforward methods for optimizing the uniaxial-film compensated WVA LCDs.

References

[1] M. Schadt and W. Helfrich, "Voltage-dependent optical activity of a twisted nematic liquid crystal," *Appl. Phys. Lett.*, vol. 18, pp. 127–128, Feb. 1971.

[2] R. A. Soref, "Field effects in nematic liquid crystals obtained with interdigital electrodes," *J. Appl. Phys.*, vol. 45, pp. 5466–5468, Dec. 1974.

[3] M. Oh-e, M. Ohta, S. Aratani, and K. Kondo, "Principles and characteristics of electro-optical behavior with in-plane switching mode," in *Proc. 15th Int. Display Research Conf. (Asia Display'95)*, 1995, pp. 577–580.

[4] S. H. Lee, S. L. Lee, and H. Y. Kim, "Electro-optic characteristics and switching principle of a nematic liquid crystal cell controlled by fringe-field switching," *Appl. Phys. Lett.*, vol. 73, pp. 2881–2883, Nov. 1998.

[5] A. Takeda, S. Kataoka, T. Sasaki, H. Chida, H. Tsuda, K. Ohmuro, Y. Koike, T. Sasabayashi, and K. Okamoto, "A super-high-image-quality multi-domain vertical alignment LCD by new rubbing-less technology," *SID Dig. Tech. Papers*, vol. 29, pp. 1077–1080, 1998.

[6] K. H. Kim, K. H. Lee, S. B. Park, J. K. Song, S. N. Kim, and J. H. Souk, "Domain divided vertical alignment mode with optimized fringe field effect," in *Proc. 18th Int. Display Research Conf. (Asia Display'98)*, 1998, pp. 383–386.

[7] J. Chen, K.-H. Kim, J.-J. Jyu, J. H. Souk, J. R. Kelly, and P. J. Bos, "Optimum film compensation modes for TN and VA LCDs," in *SID Dig. Tech. Papers*, vol. 29, 1998, pp. 315–318.
[8] J. E. Anderson and P. J. Bos, "Methods and concerns of compensating in-plane switching liquid crystal displays," *Jpn. J. Appl. Phys.*, pt. 1, vol. 39, pp. 6388–6392, Nov. 2000.
[9] Q. Hong, T. X. Wu, X. Zhu, R. Lu, and S. -T. Wu, "Extraordinarily high-contrast and wide-view liquid-crystal displays," *Appl. Phys. Lett.*, vol. 86, p. 121107, Mar. 2005.
[10] Y. Saitoh, S. Kimura, K. Kusafuka, and H. Shimizu, "Optimum film compensation of viewing angle of contrast in in-plane-switching-mode liquid crystal display," *Jpn. J. Appl. Phys.*, pt. 1, vol. 37, pp. 4822–4828, Sep. 1998.
[11] T. Ishinabe, T. Miyashita, T. Uchida, and Y. Fujimura, "A wide viewing angle polarizer and a quarter-wave plate with a wide wavelength range for extremely high quality LCDs," in *Proc. 21st Int. Display Research Conf. (Asia Display/IDW'01)*, 2001, pp. 485–488.
[12] T. Ishinabe, T. Miyashita, and T. Uchida, "Wide-viewing-angle polarizer with a large wavelength range," *Jpn. J. Appl. Phys.*, pt. 1, vol. 41, pp. 4553–4558, Jul. 2002.
[13] J. E. Bigelow and R. A. Kashnow, "Poincaré sphere analysis of liquid crystal optics," *Appl. Opt.*, vol. 16, pp. 2090–2096, Aug. 1977.
[14] P. Yeh and C. Gu, *Optics of Liquid Crystal Displays*. New York: Wiley, pp. 136–155.
[15] A. Lien, "A detail derivation of extended jones matrix representation for twisted nematic liquid crystal displays," *Liq. Cryst.*, vol. 22, pp. 171–175, 1997.
[16] M. G. Robinson, J. Chen, and G. D. Sharp, *Polarization Engineering for LCD Projection*. New York: Wiley, 2005.
[17] A. Lien, "Extended Jones matrix representation for the twisted nematic liquid-crystal display at oblique incidence," *Appl. Phys. Lett.*, vol. 57, pp. 2767–2769, Dec. 1990.
[18] X. Zhu and S. T. Wu, "Super wide view in-plane switching LCD with positive and negative uniaxial a-films compensation," in *SID Dig. Tech.Papers*, vol. 34, 2005, pp. 1164–1167.
[19] R. Lu, X. Zhu, S. T. Wu, Q. Hong, and T. X. Wu, "Ultrawide-view liquid crystal displays," *J. Display Technol.*, vol. 1, pp. 3–14, Sep. 2005.
[20] P. G. de Gennes and J. Prost, *The Physics of Liquid Crystals*, 2nd ed. New York: Oxford Univ. Press, 1995, ch. 3.

Xinyu Zhu received the B.S. degree from Jilin University, China, in 1996, and the Ph.D. degree from Changchun Institute of Optics, Fine Mechanics and Physics, The Chinese Academy of Sciences, China, in 2001. His Ph.D. research work mainly involved the reflective liquid crystal display with single polarizer.

He is currently a research scientist at the College of Optics and Photonics, University of Central Florida, Orlando. His current research interests include reflective and transflective liquid crystal displays, liquid-crystal-on-silicon projection display, wide view liquid crystal displays, and adaptive optics application with nematic liquid crystals.

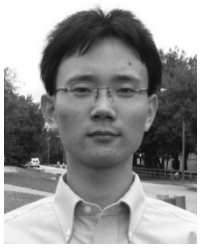

Zhibing Ge (S'02) received the B.S. degree from Zhejiang University, Hangzhou, China, in 2002, and the M.S. degree from the University of Central Florida, Orlando, in 2004, both in electrical engineering. He is currently working toward the Ph.D. degree at Department of Electrical and Computer Engineering, University of Central Florida, Orlando. His Ph.D. study concentration is in liquid crystal display modeling, transflective liquid crystal displays, and numerical analyses and optimization of liquid crystal devices.

Shin-Tson Wu (M'98–SM'99–F'04) received the B.S. degree in physics from National Taiwan University, Taipei, Taiwan, R.O.C., and the Ph.D. Degree from the University of Southern California, Los Angeles.

He is currently a PREP professor with College of Optics and Photonics, University of Central Florida, Orlando. His recent studies focus on foveated imaging, bio-photonics, laser beam steering, and LCDs. He has coauthored two books, *Reflective Liquid Crystal Displays* (Wiley, 2001) and *Optics and Nonlinear Optics of Liquid Crystals* (World Scientific, 1993).

Dr. Wu is a Fellow of the Society for Information Display (SID) and the Optical Society of America (OSA).